THE UNIVERSITY OF ALBERTA

RAY TRACING ANALYSIS OF MULTIMODE OPTICAL FIBER COMPONENTS

BY

M . SHARIF AKTARY

A THESIS

SUBMITTED TO THE FACULTY OF GRADUATE STUDIES AND RESEARCH

IN PARTIAL FULFILMENT OF THE REQUIREMENTS FOR THE DEGREE

OF MASTER OF SCIENCE

DEPARTMENT OF ELECTRICAL ENGINEERING

EDMONTON, ALBERTA

FALL 1990

National Library of Canada
Bibliothèque nationale du Canada

Canadian Theses Service
Service des thèses canadiennes

Ottawa, Canada
K1A 0N4

The author has granted an irrevocable non-exclusive licence allowing the National Library of Canada to reproduce, loan, distribute or sell copies of his/her thesis by any means and in any form or format, making this thesis available to interested persons.

The author retains ownership of the copyright in his/her thesis. Neither the thesis nor substantial extracts from it may be printed or otherwise reproduced without his/her permission.

L'auteur a accordé une licence irrévocable et non exclusive permettant à la Bibliothèque nationale du Canada de reproduire, prêter, distribuer ou vendre des copies de sa thèse de quelque manière et sous quelque forme que ce soit pour mettre des exemplaires de cette thèse à la disposition des personnes intéressées.

L'auteur conserve la propriété du droit d'auteur qui protège sa thèse. Ni la thèse ni des extraits substantiels de celle-ci ne doivent être imprimés ou autrement reproduits sans son autorisation.

ISBN 0-315-64964-X

THE UNIVERSITY OF ALBERTA

RELEASE FORM

NAME OF AUTHOR: M. SHARIF AKTARY

TITEL OF THESIS: RAY TRACING ANALYSIS OF MULTIMODE OPTICAL FIBER COMPONENTS

DEGREE FOR WHICH THESIS WAS PRESENTED: MASTER OF SCIENCE

YEAR THIS DEGREE GRANTED: FALL 1990

Permission is hereby granted to THE UNIVERSITY OF ALBERTA LIBRARY to reproduce single copies of this thesis and to lend or sell such copies for private, scholerly or scientific research purposes only.

The author reserves othe publication rights, and neither the thesis nor extensive extracts from it may be printed or otherwise produced without the author's written permission.

(SIGNED).....

PERMANENT ADDRESS:

#34 11024 88 AVE

EDMONTON, ALBERTA

T6G 0Z2

DATED.....

THE UNIVERSITY OF ALBERTA

FACULTY OF GRADUATE STUDIES AND RESEARCH

The undersigned certify that they have read, and recommend to the faculty of Graduate Studies and Research, for acceptance, a thesis entitled RAY TRACING ANALYSIS OF MULTIMODE OPTICAL FIBER COMPONENTS submitted by M. SHARIF AKTRAY in partial fulfilment of the requirements for the degree of MASTER of SCIENCE.

J.N. McMullin.
Supervisor

C.E. Capjack

W. Finlay

Date. Oct. 9, 1990

ABSTRACT

In this thesis the T-matrix method is employed for the characterization of multimode graded-index optical fiber components using geometrical optics. The components under consideration are, connectors, taps and microbending sensors.

The power loss characteristics of connectors with lateral, axial, and angular missalignments are determined. It is found that the volume occupied by the excited mode groups in the phase-space exhibits a rotational symmetry and thus, fiber connections with lateral offset and angular missalignment can be treated in the same manner.

The power attenuation characteristics of taps with respect to the distance along the bend and the radius of curvature of the bend are presented. Also, the mode stripping property of bent fibers is confirmed by calculating the modal power distributions at different points along the bend.

The characteristic behavior of loss with respect to the change in the amplitude and the period of a single microbending sensor is calculated and the resonant property of the microbending sensor is confirmed. Finally, from the analysis of serial sensors it is found that the loss in a given sensor is nearly independent of the loss in other sensors.

ACKNOWLEDGEMENT

I would like to thank Dr. J. N. McMullin for his constant support, guidance and encouragement throughout this project. Also greatly appreciated is his derivation of the ray equations by Hamiltonian mechanics for fibers with geometrical perturbation. In addition I would like to extend my sincere thanks to the following:

- the members of the examining committee.
- Mr. Goksin Bakir for his computer graphics help.
- Mr. Graham McKinnon for his assistence in computing.
- Messrs. Koon Hoo Teo and Mnoon-Yan Loke for their fruitful discussions.

Last but not least, my family and friends for their support and encouragement.

TABLE OF CONTENTS

CHAPTER		PAGE
1.	Introduction	1
	1.1 Historical Background	1
	1.2 Thesis Objective	2
	1.3 Description of the Thesis	3
	I. Connectors	3
	II. Bent fiber taps	3
	III. Microbending Sensor	4
	1.4 Organization of the Thesis	4
2.	Background Theory	7
	2.1 The Wentzel-Kramers-Brillouin (W.K.B) Approximation	7
	2.2 Ray Equations in Straight Fiber	13
	2.3 Relation Between Input and Output	17
	2.4 Numerical Method for Mode Group Excitation	21
3.	Connectors	26
	3.1 Introduction	26
	3.2 Two- Fibers with Lateral, Axial and Angular Missalignments	26
	3.3 Special Cases	30
	I. Two Fibers with Lateral Mismatch	30
	II. Two Fibers with Axial Separation	32
	III. Two Fibers with Angular Mismatch	32
4.	Bent Fiber Tap	38

4.1 Ray Equations.....38

4.2 Loss Mechanisms in a Bent Fiber.....42

4.2.1 A Method For Calculating The Loss.....43

5. Microbending Sensors.....55

5.1 Ray Equations.....55

5.2 Loss Mechanism in a Sensor.....58

5.2.1 A Method for Calculating the Loss.....59

5.3 Characteristics of Microbending Sensors.....60

5.3.1 The Modal Power Distribution.....64

5.3.2 Effect of Change in Microbending Amplitude on Power Loss.....64

5.3.3 Effect of Change in Microbending Period on Power Loss.....67

5.4 Serial Microbending Sensors.....68

6. Summary.....75

LIST OF TABLES

TABLE PAGE

2.1 Combination of i and j for type two excitation.....25

4.1 Simulation results for rays advancing along a fiber with R=8mm and λ=1.3μm.

(a) ray from mode group m=8.....47

(b) ray from mode group m=9.....47

LIST OF FIGURES

FIGURE PAGE

2.1 Graphical representation of a ray and its components.....10

2.2 Phase-space positions of descrete set of rays used for simulations.

(a) Position X and Y of the rays.....23

(b) Orientation k_x and k_y of the rays normalized to k_{1_m}.....24

3.1 Schematic diagram of two fibers with lateral, axial and angular missalignments.....27

3.2 A typical T-matrix for a lateral mismatch of 10μm.....31

3.3 Plot of loss versus lateral offset parameterized by the ratio of the radii of the second fiber to the first fiber.....34

3.4 Plot of transmission versus lareral offset parameterized by the ratio of the radii of the second fiber to the first fiber.....35

3.5 Plot of loss versus axial separation.....36

3.6 Plot of loss versus tilt angle parameterized by the transmission coefficient between the two fibers.....37

4.1 Schematic diagram of a circularly bent fiber with radius of curvature R and the rotating coordinate axis X Y Z.....39

4.2 Schematic diagram of the ray path onto the X-Y plane.....44

4.3 A typical T-matrix at a distance of three ray period along the bend.....48

4.4 Plot of loss versus normalized distance along the bend parameterized by the radius of curvature of the bend for a fiber with a = 50μm, NA = 0.159, n_1 = 1.52 and λ = 1.0μm.....50

4.5 Plot of loss versus normalized distance along the bend for a conventional fiber with a = 25μm, NA = 0.2 and n_1=1.46 and λ = 1.3μm.....51

4.6 Plot of loss versus the radius of curvature of the bend for fiber with a = 25μm, NA = 0.2, n_1=1.46 and λ = 1.3μm.....52

4.7 Plot of modal power distribution for a conventional fiber at distances of 0.1mm and and 10mm along the bend.....53

4.8 Plot of differential mode attenuation for a conventional fiber at distances of 0.1mm and 10mm along the bend.....54

5.1 Schematic diagram of a microbending sensor with period Λ and amplitude δ.....56

5.2 A typical T-matrix at a distance of 7mm along the sensor.....61

5.3 Plot of loss versus distance along a conventional fiber sensor parameterized by the amplitude of the sensor.....62

5.4 Plot of loss versus distance along a conventional fiber sensor for large distance along the sensor.....63

5.5 Plot of modal power distribution along a conventional fiber sensor at distances of 0.1, 5 and 7mm along the sensor.....65

5.6 Plot of loss versus the amplitude of the sensor

parameterized by the period of the sensor.....66

5.7 Plot of loss versus the period of the sensor for sensor amplitude δ = 1μm.....69

5.8 Schematic diagram of two serial sensors with periods Λ_1 and Λ_2, and amplitudes δ_1 and δ_2 separated by a straight section of the fiber with length l.....71

5.9 Plot of loss versus the distance along the two sensors parameterized by the amplitude of the first sensor.....73

5.10 Plot of change in the loss at the second sensor versus the loss at the first sensor for $\Lambda_1=\Lambda_2$=1.5mm.....74

SYMBOLS AND ACRONYMS

E	1. electric field
	2. Young's modulus
n_1	onaxis refractive index of the fiber core
n_2	refractive index of the cladding
Δ	relative change in refractive index
Q	rate of relative change in refractive index
a	fiber core radius
n(r)	refractive index profile of the core
r	radial position
μ	radial mode number
ν	azimuthal mode number
k_o	free space wave number
λ	free space wave length
ω	angular frequency
C_o	speed of light in free space
V	speed of light on the axis of the core
m	mode group number
M	maximum number of mode groups
h	Planck's constant
R	radius of curvature of the bend
NA	numerical apperture
MPD	modal power distribution
DMA	differential mode attenuation
W.K.B	Wentzel-Kramers-Brillouin
RP	ray period

Λ	microbending sensor period
W	microbending sensor frequency
Γ	$(2\Pi^2\delta)/\Lambda^2$
δ	microbending sensor amplitude
l	length of straight fiber separating two sensors
TL	total loss
ΔP_2	change in the loss at the second sensor
P_1	loss at the first sensor
Q_1	ray frequency
β	ray propagation constant
κ	radial component of the ray
τ	time variable
ϕ	azimuthal angle of the ray position with raspect to the X direction direction
ψ	ray vector orientation angle with respect to the radial direction

CHAPTER 1

INTRODUCTION

1.1 HISTORICAL BACKGROUND

During the last two decades the world of telecommunications has been revolutionized by the introduction of optical fibers as a medium for data transmission [1]. Improvements in the quality and the rate of data transmission have been the result of extensive research on analyzing the performance of optical fibers and optical fiber components. In Local Area Networks (LANs), where mode dependent optical fiber components dominate, particular emphasis has been put on one fundamental parameter essential to the utility of any transmission line - attenuation [2]. The primary sources of loss in a fiber are absorption (UV, IR), Rayleigh scattering, and geometrical deformation of the fiber core [3,4,5]. In this thesis the contribution of absorption and Rayleigh scattering to the loss calculation is neglected and the only source of loss is considered to be the geometrical deformation of the fiber.

Traditionally the concept of loss is the same as loss per unit length. In conventional transmission media such as wires or coaxial cables the loss can be described in terms of loss per unit length. The calculation of loss in single mode fibers follows this tradition and their loss can be defined per unit length [5,6]. However, in multimode fibers, where each mode attenuates at a different rate, the concept of a single loss per unit length is no longer valid. The nonexistence of loss

per unit length poses a serious problem for characterizing the loss behavior of multimode fibers [6]. Thus, a criterion is needed by which the loss from each mode and the total loss of multimode optical fibers and optical fiber components can be determined.

1.2 THESIS OBJECTIVE

The primary objective of this research project is to accurately determine the total loss (attenuation) of mode dependent graded index optical fiber components using geometrical optics. This task requires the development of a technique in which the loss contribution of each mode group to the total loss is considered. The mode dependent optical fiber components under consideration are connectors, taps and microbending sensors. For achieving the primary objective, some underlying theory and numerical procedures must be described. They are:

1. Description of a connection between the wave theory and the ray theory which enables us to relate rays to modes of propagation in a multimode graded index fiber.

2. Derivation of the ray equations in circularly and periodically deformed fiber which govern the dynamics of the rays inside the fiber core and determination of the solutions to the ray equations.

3. Description of a method for selecting a representative set of rays for numerical simulations of mode dependent optical fiber components [8].

4. Development of a simulation program for calculating the loss of each mode group, the distribution of power among mode groups and the total loss at any distance along the fiber.

1.3 DESCRIPTION OF THE COMPONENTS

The components under consideration in this thesis are connectors, taps and microbending sensors. These components are made of graded index fiber with a parabolic index of refraction $n(x,y) = n_1\left[1 - Q^2\left(X^2 + Y^2 \right)\right]^{1/2}$ where n_1 is the index of refraction at the center of the fiber core, $Q^2 = \frac{2\Delta}{a^2}$ with $2\Delta = \frac{(n_1^2 - n_2^2)}{n_1^2}$, a is the core radius of the fiber and n_2 is the cladding index of refraction.

I. *Connectors:* In optical communication networks such as LANs concatenation of fibers is inevitable. Connector is the name given to any device used to join two fibers [7]. Due to the small dimension of fibers' cores, it is almost impossible to achieve a perfect connection and hence, impossible to avoid the loss of optical power and coupling of power among mode groups [7]. The amount of loss in a connector depends on the degree of misalignment of the two fibers' cores [7]. A better knowledge of the loss due to the insertion of connectors in an optical communication network leads to cost efficient design of the network. Chapter 3 is devoted to the study of connectors.

II. *Bent fiber taps:* In this thesis, a tap is considered to be a mechanically stressed (bent) fiber [8]. Taps are primarily used for extracting a small amount of optical power from a fiber for purposes such as distributing power to a large number of nodes, CATV distribution and optical clock distribution in LANs [9]. Furthermore, bending of the fiber gives rise to loss of optical power from the fiber core which can be measured by an optical time domain reflectometer (OTDR) [6]. A property of the bent fibers is that higher order modes are eliminated from the fiber core when the fiber is wrapped around a mandrel [10].

This property can be used for the purpose of launching light power with fewer number of modes into another fiber.

The amount of light power extracted from the bent fiber depends on the radius of curvature of the bend. That is, the smaller the radius of the bend the larger the extracted power will be. A detailed analysis of the bent fibers is provided in chapter 4 of this thesis.

III. *Microbending sensor*: A microbending sensor is a periodically perturbed fiber characterized by its amplitude, its period and the number of periods in its total length [11]. A simple procedure for producing a microbending sensor is by pressing a fiber between two plates with periodic deformation. As in the case of a single bend, microbending of the fiber gives rise to loss of optical power from the fiber core which can be detected by an (OTDR) [12]. This desirable property of the microbend allows it to be used as a device for sensing pressure [13] sound levels [14,15], displacement [16] and structural distortions [17]. Henceforth, in this thesis, the word sensor will always mean microbending sensor. A detailed description of the characteristics of a single sensor and sensors in series is given in chapter 5 of this thesis.

1.4 ORGANIZATION OF THE THESIS

Chapter 2 of this thesis provides a full description of the theory employed to achieve the objectives of this research project. In this chapter the connection between the ray optics and the wave optics is reviewed using the semiclassical W.K.B. approximation. Then the ray equations of motion for a multimode straight fiber with parabolic index of refraction are derived using Hamiltonian mechanics. The solutions to

the ray equations as functions of the distance along the fiber are obtained and are used to assign the rays to modes of propagation. Finally a technique is devised to relate the input power to the output power through a matrix called the T-matrix.

Chapter 3 is devoted to the study of connectors. The ray position and orientation emerging from one fiber are related to the ray position and orientation entering the second fiber for a general configuration of lateral, axial and angular misalignment. Then the T-matrix is determined from which the total loss is found. Then for the purpose of comparing the result to other publications, special cases of the two fiber misalignments are considered.

Chapter 4 provides a detailed analysis of bent fibers. The equations of motion for the rays in a bent fiber with constant radius of curvature are derived. The solutions to the ray equations in terms of the distance along the bend are obtained. Next, the loss mechanisms are introduced and the procedure for determining the T-matrix is given. The characteristic behavior of loss versus the distance along the bend and loss versus the radius of curvature of the bent fiber are discussed. Then the results are compared with other publications on bent fibers.

Chapter 5 is devoted to the study of sensors and the results are compared to published experimental and theoretical work. In this chapter the solutions to the ray equations are obtained in a fiber with a sinusoidal deformation of the axis. Then the loss mechanisms are introduced and the procedure for determining the T- matrix is outlined. The characteristic behavior of loss versus the distance along the sensor is discussed. The effects of the change in the amplitude and the period of the sensor on the loss are discussed and the resonant property of the

sensor is observed. Next, the performance of serial sensors is studied. More emphasis has been put on the performance of the second sensor while the first sensor is subjected to amplitude changes. This chapter may be considered the first original research for analyzing microbending sensors using ray theory.

A summary and conclusions are provided in chapter 6.

CHAPTER 2

BACKGROUND THEORY

2.1 THE WENTZEL-KRAMERS-BRILLOUIN (W.K.B) APPROXIMATION

The propagation of visible and infrared light (electromagnetic waves) is characterized by very high frequency (of the order 10^{14}/sec) and short wavelength (of the order 10^{-6}m) [18]. In optical fiber communications we are often concerned with optical fibers and optical fiber components of much larger dimensions than the wavelength of the visible light. For example, a conventional multimode graded index fiber has a core radius a=25μm and a change in the index of refraction much smaller than unity in a distance compared to one wavelength [19,20], i.e $\lambda \left|dn(r)/dr\right| \ll 1$. This fact allows for an approximation to the propagation laws of light by a complete neglect of the wave length [18]. This approximation which replaces wave theory of visible light by classical theory of a point particle is called geometrical optics [18]. The optical energy is regarded as being transported along curves called light rays. Before commencing a rigorous analysis of the optical fiber components by geometrical optics (ray optics) theory, let us first review the connection between wave optics and ray optics [18].

In wave theory, a mode of propagation in a graded index fiber is an eigenfunction of Maxwell's equations belonging to a particular eigenvalue (propagation constant) and satisfying all the boundary conditions [21]. The modes are traveling waves along the fiber axis (in the Z direction) that are composed of superimposed traveling waves which

together form a standing wave pattern in the radial (transverse) direction. A mode of propagation in the W.K.B approximation is assumed to have the following form [21]

$$E(r, \phi, Z)=A(r) \exp\left\{i\left[\omega t - S(r, \phi, Z)\right]\right\} \qquad (2.1)$$

where $E(r, \phi, Z)$ is the electric field, ω is the frequency, $A(r)$ is the slowly varying amplitude of the electric field. The spatial argument of the above exponential function which describes the phase front of a propagating mode can be written as follows

$$S(r, \phi, Z) = F(r) + \nu\phi + \beta Z \qquad (2.2)$$

where $r = (X^2 + Y^2)^{1/2}$, ν is the azimuthal mode number, ϕ is the azimuthal angle, β is the propagation constant, and $F(r)$ is the slowly-varying phase function.

On the other hand, rays are defined as those curves which are perpendicular to the phase front of the propagating mode. Thus, a ray can be described by the gradient of the phase front as follows [18]

$$\nabla S(r, \phi, Z)= \bar{k}(r) = \frac{dF(r)}{dr}\,\hat{r} + \frac{\nu}{r}\,\hat{\phi} + \beta\,\hat{Z} \qquad (2.3)$$

where $\bar{k}(r)$, the ray vector, gives the local direction of propagation and the wavelength of the light through the relation $\lambda = \frac{2\pi}{|\bar{k}(r)|}$. The W.K.B. approximation provides an expression for the derivative of $F(r)$ as follows [18]

$$\kappa = dF(r)/dr = \left[n^2(r)k_o^2 - \beta^2 - (\nu/r)^2\right]^{1/2} \qquad (2.4)$$

and hence,

$$| k(r) |^2 = n^2(r)k_o^2 = \kappa^2 + (\nu/r)^2 + \beta^2 \qquad (2.5)$$

where k_o is the free space wave vector and n(r) is the refractive index which has the following form.

$$n(X,Y) = n_1\left[1 - 2\Delta\left(\frac{X^2+Y^2}{a^2}\right)\right]^{1/2} \qquad (2.6)$$

Eq. (2.5) indicates that a ray in a fiber is the same as the wave vector of a propagating mode with propagating constant β. A ray and its components are shown in Fig. 2.1. This figure shows that κ, ν/r_o and β are the radial, azimuthal and longitudinal components of the ray respectively. They can be written as follow

$$\beta \cong n(r)\, k_o\, \mathrm{Cos}\theta \qquad (2.7)$$

$$\kappa = n(r)\, k_o\, \mathrm{Sin}\theta\, \mathrm{Cos}\psi \qquad (2.8)$$

$$\nu = r\, n(r)\, k_o\, \mathrm{Sin}\theta\, \mathrm{Sin}\psi \qquad (2.9)$$

where θ is the angle between the ray and the fiber axis inside the fiber and ψ is the angle that the projection of the ray onto the fiber's cross section makes with the radial direction.

Another important result of the W.K.B. approximation is the

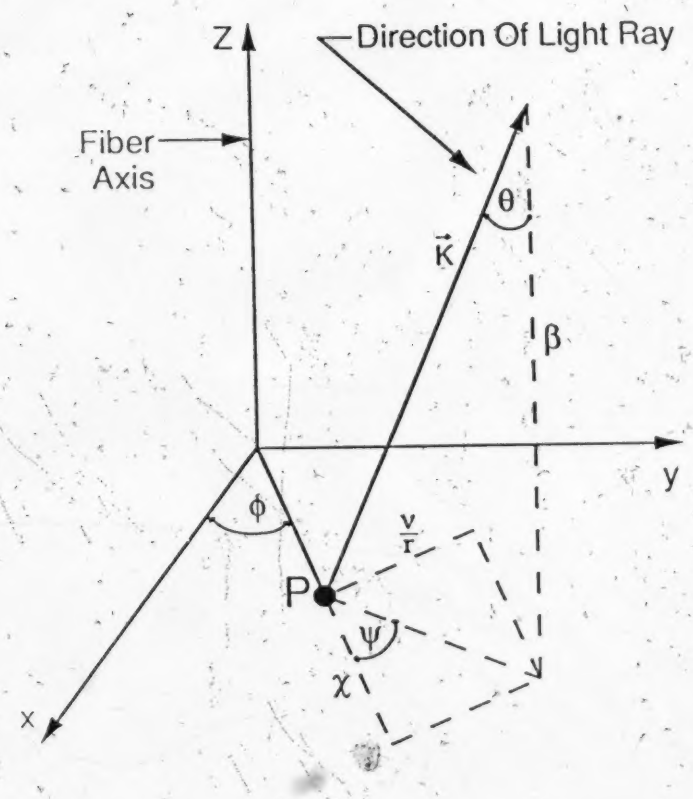

Fig.2.1 A schematic diagram of a ray and its components.

determination of the eigenvalue β of a propagating mode in terms of its radial μ and azimuthal ν mode numbers. The result is quoted here [21]

$$\beta = n_1 k_o \left[1 - 2(2\Delta)^{1/2} \left\{ \frac{2\mu + \nu + 1}{n_1 k_o a} \right\} \right]^{1/2} \qquad (2.10)$$

where $\Delta = \dfrac{n_1^2 - n_2^2}{2n_1^2}$ with n_1 being the on axis index of refraction and n_2 being the cladding index of refraction. A mode of propagation is represented by a pair of μ and ν. An interesting observation which can be made from Eq. (2.10), is that there are many modes (eigenfunctions) corresponding to the same β (eigenvalue). These modes with the same β constitute a *mode group* whose propagation constant is labelled by an integer $m = 2\mu + \nu + 1$ as follows [21].

$$\beta_m = n_1 k_o \left[1 - 2\Delta \frac{m}{M} \right]^{1/2} \qquad (2.11)$$

Where m is called the mode group number and M is the total number of guided mode groups supported by the fiber. The value of M depends on the free space wave number and fiber's parameters such as a (core radius) and NA (numerical aperture) as $M = 1/2\ (k_o\ a\ NA)$.

However, not all the modes in a fiber are guided modes. There are three types of modes in a fiber, classified by their value of m [21]. All those modes with $m < M$ are classified as guided modes [22,23]. All those modes with $M < m < 2M$ are classified as leaky modes. They are called leaky because they gradually radiate power from the fiber core as they advance along the fiber. All those modes with $m > 2M$ are classified as radiation modes and are considered to be the major contributor to the

power loss from the fiber core though coupling of power from guided modes to radiation modes. A detailed description of the mode classification is given in Reference [21].

So far the W.K.B. approximation has paved the way to establishing a connection between rays and modes. We are now prepared to derive an expression which will serve as the most important relation in ray optics of graded index fiber. From Eqs. (2.7) through (2.9) a relation between the propagation constant β and the ray orientation with respect to the fiber axis is obtained as follows [3]

$$\beta = k_o \left[n^2(r) - \mathrm{Sin}^2\theta_o \right]^{1/2} \qquad (2.12)$$

where θ was replaced by θ_o through Snell's law $n(r)\mathrm{Sin}\theta = \mathrm{Sin}\theta_o$, with θ_o being the angle between k(r) and the Z axis where the ray enters into or emerges from the fiber end face. Comparing Eq. (2.11) with Eq. (2.10) gives [3]

$$\frac{m}{M} = \left(\frac{r}{a}\right)^2 + \left(\frac{\sin\theta_o}{\sin\theta_c}\right)^2 \qquad (2.13)$$

where $\mathrm{Sin}\theta_c = n_1(2\Delta)^{1/2}$ and $r^2 = X^2 + Y^2$ is the radial distance from the fiber axis. For convenience in the following sections, Eq. (2.13) can be written as follows [8]

$$\frac{m}{M} = \left(\frac{r}{a}\right)^2 + \left(\frac{k_\perp}{k_{\perp_m}}\right)^2 \qquad (2.14)$$

where $k_\perp = k_o \mathrm{Sin}\theta_o$ is the projection of the ray onto the fiber cross

section and is given in terms of k_x and k_y as follows

$$k_\perp^2 = k_x^2 + k_y^2 \qquad (2.15)$$

and $k_{\perp_m} = k_o NA$ is the maximum allowable value of $k_\perp$.

Equation (2.13) establishes the foundation for the principle of mode group excitation and detection in a fiber by rays [3]. According to Eq. (2.13), a particular mode group can be excited in a fiber by rays, provided that the position r and the orientation $k_\perp$ of the rays with respect to the fiber axis satisfy Eq. (2.14).

The next step is the derivation of the ray equations. The ray equations allow for the determination of the instantaneous position and orientation of the rays along the fiber and thus enable us to assign a ray to a particular mode group at any point along the fiber.

2.2 RAY EQUATIONS IN STRAIGHT FIBER

The ray equations can be derived from the W.K.B theory [21]. It is found that [18]

$$(\nabla S)^2 = n^2(\bar{x}) \qquad (2.16)$$

where $\bar{x}$ is the position and S, the eikonal, is the surface of constant phase which defines the shape of the radiation field and ∇ is the gradient operator. Hence, the eikonal equation may be used to determine the propagation of waves in geometrical optics approximation [21]. However, it is more desirable to calculate the ray equations directly without having to construct the phase fronts using the eikonal equation.

This can be achieved from the eikonal equation by defining a fixed point as the origin and drawing a vector $\bar{r}$ from the origin to all the points along the ray. By defining s as the distance along the ray, a unit vector $\bar{u}$ may be obtained as

$$\bar{u} = \frac{d\bar{r}}{ds} \tag{2.17}$$

Knowing that a ray is perpendicular to the phase front S, then another vector may be defined as

$$\bar{v} = \nabla S \tag{2.18}$$

where the magnitude of the v vector is determined from the eikonal equation to be $|v| = n$. The vectors u and v are required to be parallel, thus the ray equation is determined to be [21]

$$d/ds(n(\bar{x})\ d\bar{x}/ds) = \nabla n(\bar{x}) \tag{2.19}$$

where $\bar{x}$ is the position, s is the distance along the ray and $n(\bar{x})$ is the index of refraction.

An alternative procedure is the Hamiltonian formulation of geometrical optics [8] which yields the same result as the previous approach even though the starting assumptions are different. In this approach a ray is perceived as the trajectory of a photon which can be treated as a quantum mechanical particle [26]. It is well-known that the energy and the momentum of a photon are related to its frequency ω and wave vector $\bar{k}(\bar{r})$ by [20]

$$E = \frac{h}{2\pi}\,\omega(\bar{x},\ \bar{k}) \tag{2.20}$$

$$\bar{P} = \frac{h}{2\pi}\,\bar{k} \tag{2.21}$$

where h is the Planck's constant. The dispersion relation which relates the frequency ω to the wave vector $\bar{k}$ may be derived from Maxwell's equations in the medium [25]. In an optical medium such as glass, a good approximation for the dispersion relation is

$$\omega(x,\ k) = \frac{C_o k}{n(x)} \tag{2.22}$$

where C_o is the speed of light in free space. Hence, the photon energy E may be written as

$$E = \frac{C_o \bar{P}}{n(x)} \tag{2.23}$$

Hamilton's equations of motion are defined as [27,28]

$$\dot{\bar{X}} = \frac{\partial E}{\partial \bar{P}}$$

$$\dot{\bar{P}} = -\frac{\partial E}{\partial \bar{X}}$$

where the dot represents differentiation with respect to time t. Hence, the following equations of motion are obtained

$$\frac{d\bar{X}}{d\tau} = \frac{C_o^2 \bar{k}}{\omega} \tag{2.24}$$

$$\frac{d\bar{k}}{d\tau} = (\omega/2)\,\nabla n^2(X) \qquad (2.25)$$

where the variable τ is defined as $\tau = \int dt/n^2(X)$. From the Z component of Eq. (2.24) a relation between Z and τ can be obtained as follows

$$Z = \frac{C_o^2 k_z \tau}{\omega} + Z_o \qquad (2.26)$$

where $k_z = \beta$ and from the previous section $\beta = n_o k_o (1 - 2\Delta \frac{m}{M})^{1/2}$. Choosing $Z_o = 0$, the solutions for the X, Y, k_x, and k_y components of Eq. (2.24) and (2.25) can be written as a function of the distance along the fiber axis as follows.

$$X(Z) = X_o \mathrm{Cos}(Q_1 Z) + (k_{xo}/n_1 k_o Q)\,\mathrm{Sin}(Q_1 Z) \qquad (2.27)$$

$$Y(Z) = Y_o \mathrm{Cos}(Q_1 Z) + (k_{yo}/n_1 k_o Q)\,\mathrm{Sin}(Q_1 Z) \qquad (2.28)$$

$$k_x(Z) = k_{xo}\mathrm{Cos}(Q_1 Z) - X_o n_1 k_o Q\,\mathrm{Sin}(Q_1 Z) \qquad (2.29)$$

$$k_y(Z) = k_{yo}\mathrm{Cos}(Q_1 Z) - Y_o n_1 k_o Q\,\mathrm{Sin}(Q_1 Z) \qquad (2.30)$$

where $Q^2 = \frac{2\Delta}{a}$, $Q_1 = \frac{Q}{(1 - 2\Delta \frac{m}{M})^{1/2}}$, $r^2(Z) = X^2(Z) + Y^2(Z)$, $k_x(Z)$ and $k_y(Z)$ are the X and Y components of the k vector, k_{xo} and k_{yo} are the initial X and Y components of the k vector and X_o and Y_o are the x and y coordinate of the ray at Z=0. From Eqs. (2.14) and (2.27) through (2.30), different mode groups can be excited provided that the initial conditions are selected properly [29,30]. In Section 2.5 a numerical technique is described which enables us to excite (at the fiber input) and identify (at the fiber output) mode groups by rays.

The substitution of Eqs. (2.27) through (2.30) into Eq. (2.14)

confirms the conservation of the mode group number (m = constant) for a ray travelling along a straight fiber.

2.3 RELATION BETWEEN INPUT AND OUTPUT POWER

In a transmission line, power as a function of the distance Z is described by $P(0)\exp(-\alpha Z)$ where $P(0)$ is the initial power and α is the attenuation coefficient. This exponential expression is also suitable for describing the power attenuation of a single mode fiber (a fiber which can support one mode) or any given mode of a multimode fiber. However, for a fiber carrying more than one mode the total power flow cannot be described by the above exponential expression [6]. This is due to the fact that every mode decays at a different rate. References 3 and 31 indicate that the attenuation rate for higher order modes is higher than that of lower order modes.

The sources of power attenuation in a fiber are absorption (UV, IR), Rayleigh scattering and geometrical perturbations of the fiber core[31]. Attenuation due to absorption results in the conversion of optical power into heat. As for Rayleigh scattering and geometrical perturbations of the fiber core, the mechanism for the loss of optical power from the fiber core is coupling of power from guided to radiation modes [31]. A small degree of mode coupling between lower order modes (low loss mode groups) to higher order modes (high loss mode groups) leads to a significant loss of power from the fiber core. Hence, for the purpose of calculating the total power attenuation in a multimode fiber we need to calculate the differential mode attenuation (DMA) [3,31]. In a strict sense, DMA is the loss of power from a single mode group to other mode groups or to radiation outside the core by means of coupling [4]. In

this thesis the effects of absorption and Rayleigh scattering are neglected and the only source of attenuation is considered to be the geometrical deformation of the fiber core or misalignment of two fibers connector.

We now proceed to develop a technique which relates the input and the output powers of the optical fiber components. Let us consider a fiber with geometric irregularities such as concatenation or deformation and in the interest of simplicity let us suppose that the fiber is excited by three mode groups and each mode group contains a certain number of rays . The geometrical irregularity of the fiber causes the rays in all mode groups to change their position and orientation with respect to the fiber axis as they advance along the fiber. By doing so some of the rays leave the mode groups to which they belonged at the input and couple to different mode groups at the output. Thus, the power of each mode group at the output is composed of the fractional powers of all the mode groups at the input. For a fiber which can support three mode groups, the powers of each mode group at the output can be written as a linear sum of the fractions of mode group powers at the input [32]. For a fiber with geometric irregularities the number of occupied mode groups at the output may not be the same as in the input. This is due to the fact that all those rays whose mode group numbers m satisfy is $M < m < 2M$ become leaky and belong to leaky mode groups. Those rays with $m > 2M$ immediately leave the fiber core and are considered lost. Hence, the powers of all the mode groups at the output can be related to the powers of all the mode groups at the input through a matrix called the T-matrix

$$\begin{bmatrix} P_1 \\ P_2 \\ P_3 \\ P_4 \\ P_5 \end{bmatrix}_{OUT} = \begin{bmatrix} T_{11} & T_{12} & T_{13} \\ T_{21} & T_{22} & T_{23} \\ T_{31} & T_{32} & T_{33} \\ T_{41} & T_{42} & T_{43} \\ T_{51} & T_{52} & T_{53} \end{bmatrix} \begin{bmatrix} P_1 \\ P_2 \\ P_3 \end{bmatrix}_{IN} \qquad (2.31)$$

Eq. (2.31) shows that the number of mode groups at the output is larger than the number of mode groups at the input. This is an indication of the fact that a fraction of the input power is transferred to the leaky mode groups (P_4) and radiation (P_5) mode groups at the output. The term radiation mode groups stands for those rays which leave the fiber core and form mode groups with mode group number m > 2M. For example, T_{51} represents the fraction of power from mode group one (at the input) that is coupled to the radiation mode groups. The DMA can be obtained from those elements of the T-matrix where i=j, as DMA= T_{jj} [4]. The rest of the elements of the T-matrix represent coupling of power among mode groups. For instance, the element T_{42} marks the ratio of the fraction of power in mode group four (leaky modes) at the output that is converted from mode group two at the input to the power of mode group two at the input [32].

The T-matrix also provides information about the distribution of power among mode groups [33,34] by summing the elements of each column. The sum of each column of the T-matrix at the point of observation represents the coefficient of power which remains in a mode group (at the input) representing that column. For instance, if the sum of the elements of column three is 0.5, it will mean that mode group number

three has lost fifty percent of its initial power. The fiber under consideration in this thesis is a conventional one with core radius a=25μm, NA=0.2 and on-axis refractive index n_1=1.46. Choosing the wave length to be λ = 1.3μm, the fiber can support twelve mode groups (M=12). Hence, with full excitation of the deformed fiber at the input, the T-matrix at the output will contain twelve columns and more than twelve rows which includes the leaky mode groups. Radiation mode groups will not be included in the T-matrix. The amount of power remaining in the core at the output is obtained by following expression.

$$TL = -10 \log \left[\frac{\sum_{m1} NR(m_1) \sum_{m2} T(m_2, m_1)}{TNR} \right]$$

Where NR(m_1) is the number of rays in mode group m_1 and TNR is the total number of rays at the input.

The idea of using a matrix to determine the DMA and total loss of a multimode optical fiber was first introduced by Holms [35] and later put into practice by Evers. The matrix was called the mode transition matrix (MTM) [32]. However, in deriving the MTM an assumption was made which compromised the accuracy of this method. The division of all mode groups in a fiber into a fewer number of super mode groups, which lead to a smaller dimension matrix, was based on the assumption that all mode groups in a supermode group have the same propagation constant. Hence, the elements of the MTM provides information about DMA and coupling coefficients among supermode groups but not mode groups. The other shortcoming of the MTM is that it does not provide information about the

distribution of power among mode groups. Thus, for more accurate results the T-matrix is more useful than the MTM.

In the following chapters the T-matrix will be used to determine the total loss, DMA, modal power distribution, and mode group coupling coefficients of different optical fiber components.

2.4 NUMERICAL METHOD FOR MODE GROUP EXCITATION

To determine mode mixing and loss we perform numerical simulation of rays propagating through optical fiber components. Each mode contains a continuous set of rays satisfying the following equation.

$$\frac{m}{M} = \left(\frac{r}{a}\right)^2 + \left(\frac{k_\perp}{k_{\perp_m}}\right)^2 \qquad (2.32)$$

For the purpose of numerical simulation we replace the continuous set of rays distributed nearly uniformly in phase-space. The selection of discrete set of ray for simulations may be made as follows [8]

$$r_i = a\,(i/M)^{1/2} \qquad (2.33)$$

where i=0.5, 1.5, 2.5,...,M-0.5. Similarly $k_\perp$ can be varied as

$$k_{\perp_j} = k_{\perp^m}\,(j/M)^{1/2} \qquad (2.34)$$

where j=0.5, 1.5, 2.5,...M-i. Substitution of Eqs. (2.33) and (2.34) in Eq. (2.32) gives

$$m = i + j \qquad (2.35)$$

Thus, r and $k_\perp$ can be varied according to Eqs. (2.33) and (2.34) and the mode group number will be given by Eq. (2.35). Hence, there will be m combinations of i and j which will satisfy Eq. (2.35). The phase space can be divided according to Eq. (2.33) and (2.34) into rings. There will

be m rings in each r and $k_\perp$ spaces. Uniform distribution of the rays further requires the angular division of the rings in phase space. Let us suppose there are *l* angles (ϕ) for each ring of r and *l* angles (ψ) for each ring of $k_\perp$ chosen as follows

$$\phi_q = \psi_q = \frac{q\ 2\pi}{l} \qquad (2.36)$$

where q = 1, 2,.....*l*. For an arbitrary value of *l* the X_o, Y_o, k_{xo} and k_{yo} of a ray can be determined as follows

$$X = r_i \cos(\phi_q) \quad , \quad Y = r_i \sin(\phi_q)$$

$$k_x = k_{\perp_j} \cos(\psi_q) \ , \ k_y = k_{\perp_j} \sin(\psi_q).$$

Typical values of X_o, Y_o, k_{xo} and k_{yo} are depicted in Fig.2.2a and 2.2b. With *l* rays for each (X_o, Y_o) position and (k_{xo}, k_{yo}) orientation the total number of rays will be m $(\frac{m+1}{2})l^2$. As mentioned before the value of *l* is arbitrary. However, a larger value of *l* presumably leads to greater accuracy of the simulation results. The first choice of i and j given above leads to the excitation of bound mode groups and the second choice of i=0.5, 1.5...M-0.5 and j=0.5, 1.5...M-0.5 leads to the excitation of bound and leaky mode groups. The following example further clarifies this concept. In order to fully excite a fiber which can support 5 mode groups the possible combinations of i and j are shown in table.2.1. All the numbers inside the table represent the mode group numbers m which include bound ($m \leq 5$) and leaky ($5 < m < 9$) mode groups. This type of excitation corresponds to the second choice of i and j. All mode group numbers above and including the diagonal elements (represented by the number 5) are bound mode groups and correspond to the first choice of i and j.

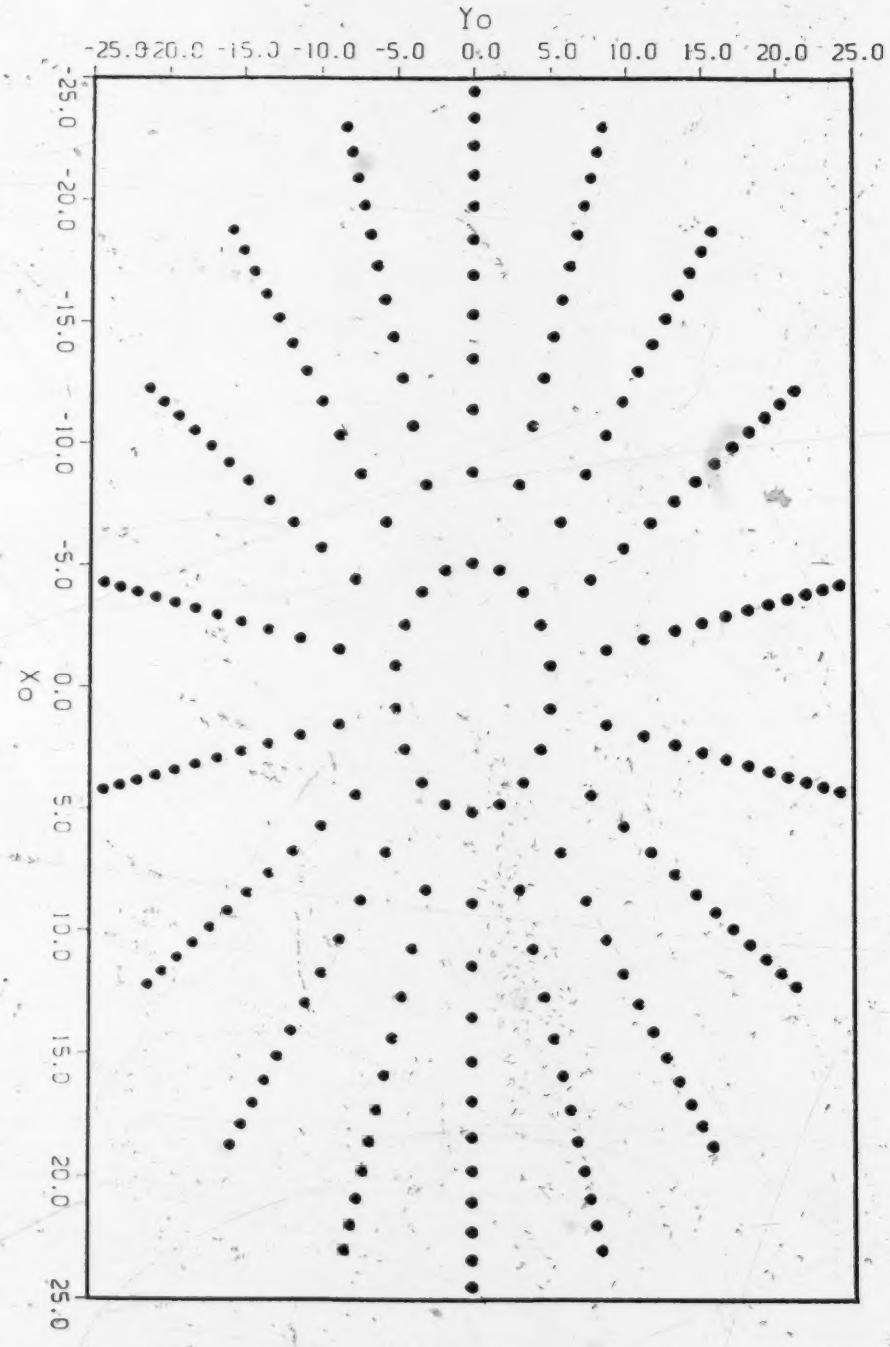

Fig. 2.2a The position X_o and Y_o of the rays.

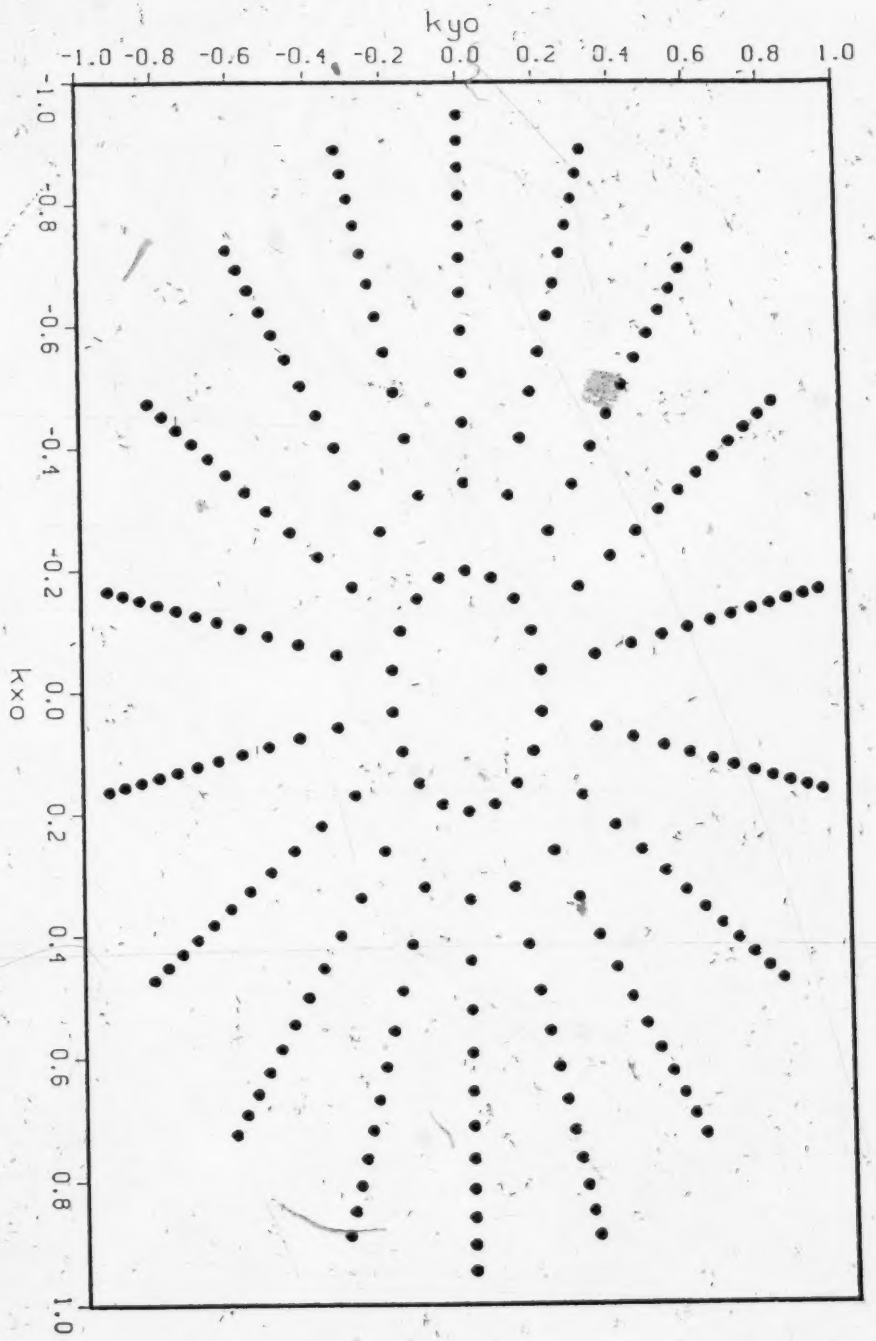

Fig.2.2b The orientation k_{xo} an k_{yo} of the rays.

In the following chapters extensive use of the above technique will be made to excite and detect mode groups at the input and at the output respectively.

j \ i	0.5	1.5	2.5	3.5	4.5
0.5	1	2	3	4	5
1.5	2	3	4	5	6
2.5	3	4	5	6	7
3.5	4	5	6	7	8
4.5	5	6	7	8	9

Table.2.1 Combinations of i and j for type two excitation.

CHAPTER 3

CONNECTORS

3.1 INTRODUCTION

A connector, in optical fiber communication, is a device which connects the end faces of two fibers [7]. Due to the small dimension of the fibers' cores, a perfect alignment of the fibers is almost impossible [36]. A number of techniques have been suggested to achieve lateral alignment between the two fibers' cross sections which includes the outer diameter of the fibers [37,38,39]. However, the alignment of the fibers' cores is not guaranteed by these techniques. This mismatch of the fibers' core crossections gives rise to the loss of power. It is the purpose of this chapter to accurately determine the amount of loss in the following misalignment configurations of two fibers.

3.2 TWO FIBERS WITH LATERAL, AXIAL AND ANGULAR MISMATCHES

A general configuration of two misaligned fibers is depicted in Fig.3.1. D_1 and D_2 are the lateral misalignments in the x and y directions respectively, D_3 is the axial separation in the z direction and α is the angular misalignment of the two fibers' axes. The direction of the power flow is from fiber one (on the left) to fiber two (on the right). Hence, the cross sectional surfaces of fiber one and fiber two are regarded as the input and the output respectively.

The amount of power at the input is determined by the number of rays emanating from the first fiber and the amount of power at the output is determined by the number of rays entering the second fiber.

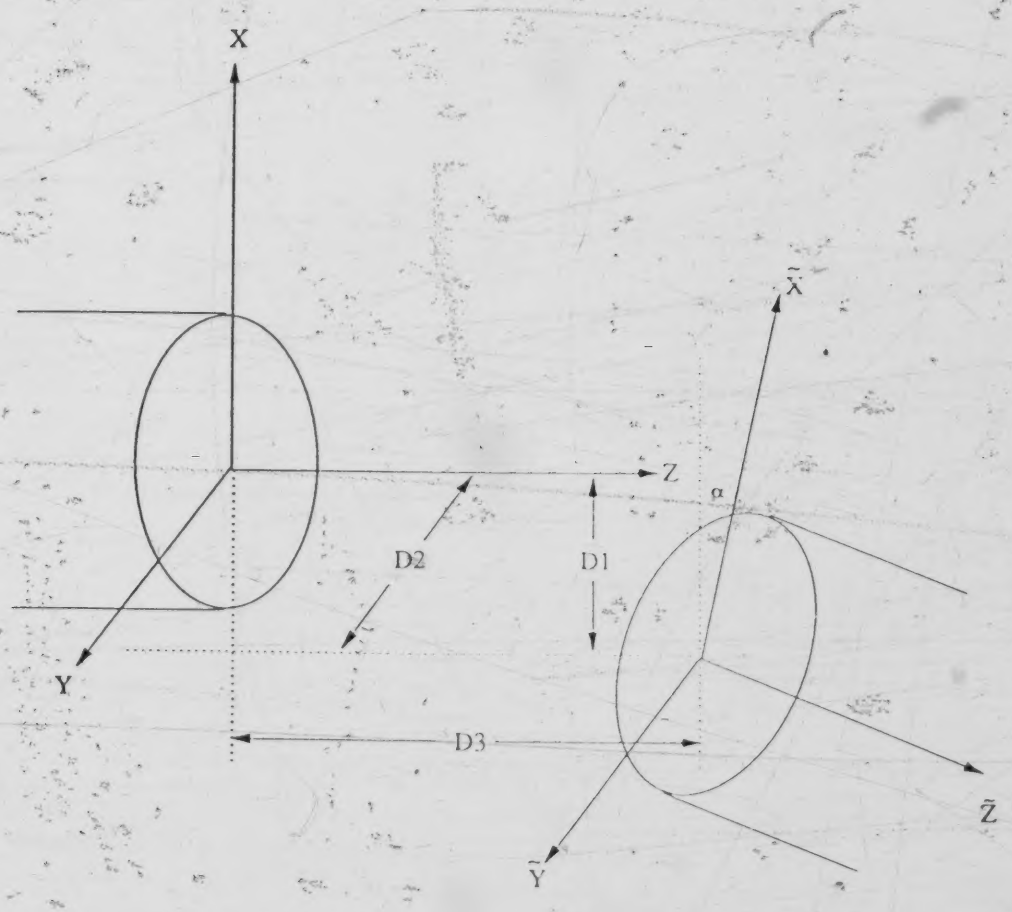

Fig.3.1 A schematic diagram of two fibers with lateral axial and angular misalignments.

To find the total loss incurred due to the misalignment of the two fibers, we need to determine the T-matrix which was introduced in Chapter 2. At the input the method introduced in Section (2.5) can be employed to generate a set of rays representing all the mode groups. Each ray has a different position and orientation with respect to the fiber two which is calculated below and then m2 can be found using Eq. (2.14).

With the connection configuration of Fig. 3.1, consider a ray emanating from the first fiber with position $(X_o, Y_o, 0)$ and orientation (k_{xo}, k_{yo}, k_{zo}). To find the position and orientation of this ray at the second fiber, there are three transformations involved. The first transformation is a translation along the z axis by a distance D_3, and the new coordinate system is called (X', Y', Z'). The ray vector in this coordinate system is

$$X' = X_o + z\,(k_{xo}/k_z) \tag{3.1}$$

$$Y' = Y_o + z\,(k_{yo}/k_z) \tag{3.2}$$

$$Z' = z - D_3 \tag{3.3}$$

where z is the distance along Z'. The second transformation involves two translations along the X' and Y' axes by distances of D_1 and D_2 respectively. This new coordinate system is called (X'', Y'', Z''). The ray vector in this coordinate system is

$$X'' = X' - D_1 \tag{3.4}$$

$$Y'' = Y' - D_2 \tag{3.5}$$

$$Z'' = Z' \tag{3.6}$$

The last transformation is a rotation and for convenience is chosen to

be around Y" axis by an angle α. The resultant coordinate system is called $(\tilde{X}, \tilde{Y}, \tilde{Z})$. The ray vector in this coordinate system is obtained as follows [40]

$$\begin{bmatrix} \tilde{X} \\ \tilde{Y} \\ \tilde{Z} \end{bmatrix} = \begin{bmatrix} \cos\alpha & 0 & \sin\alpha \\ 0 & 1 & 0 \\ -\sin\alpha & 0 & \cos\alpha \end{bmatrix} \begin{bmatrix} X_o + pz - D_1 \\ Y_o + qz - D_2 \\ z - D_3 \end{bmatrix} \tag{3.7}$$

where $p = k_{xo}/k_z$, $q = k_{yo}/k_z$. Thus

$$\tilde{X} = \frac{X_o + pD_3 - D_1}{\cos(\alpha) - p\sin(\alpha)} \tag{3.8}$$

$$\tilde{Y} = Y_o + q\left\{\frac{\sin(\alpha)\left(X_o - D_1\right) + D_3\cos(\alpha)}{\cos(\alpha) - p\sin(\alpha)}\right\} - D_2 \tag{3.9}$$

The orientation of the ray can be determined by only a rotational transformation [40], the result is given below.

$$\tilde{k}_x = k_{xo}\cos\alpha + k_{zo}\sin\alpha \tag{3.10}$$

$$\tilde{k}_y = k_{yo} \tag{3.11}$$

$$\tilde{k}_z = -k_{xo}\sin\alpha + k_{zo}\cos\alpha \tag{3.12}$$

with $k_{xo} = n(r)k_o\sin\theta\cos\psi$, $k_{yo} = n(r)k_o\sin\theta\sin\psi$ and $k_{zo} = n_1k_o(1 - 2\Delta m/M)^{1/2}$ where $k_o = 2\pi/\lambda$ is the free space wave number, $n(r)$ is the index of refraction, m is the mode group number to which the ray belongs at the first fiber and M is the total number of mode groups supported by

the first fiber.

Having determined the position and orientation of the ray at the cross section of the second fiber, the ray can now be assigned to a certain mode group by the following relation derived in Chapter 2

$$\frac{m}{M} = \left(\frac{\tilde{r}}{a}\right)^2 + \left(\frac{k_\perp}{k_{\perp_m}}\right)^2 \qquad (2.14)$$

where $\tilde{r} = (\tilde{X}^2 + \tilde{Y}^2)^{1/2}$ and $\tilde{k}_\perp = (k_{\tilde{x}}^2 + k_{\tilde{y}}^2)^{1/2}$. The same procedure is applicable to all the rays.

This procedure enables us to find the T-matrix from which the total loss, mode group coupling coefficients and modal power distribution can be obtained. The following special cases provide a better insight into the properties of misaligned fiber connections.

3.3 SPECIAL CASES

I. *Two fibers with lateral mismatch*: This is a special case of the general formulation derived in Section (3.2) of this chapter. A typical T-matrix for a connector with only lateral mismatch of D_1=10μm is given in Fig.3.2. The number at the bottom of the T-matrix represents the total loss which was determined by the expression given in Chapter 2. The total loss obtained from the T-matrix is in good accord with that of Reference 7 which uses the MTM. Knowing that all mode groups at the first fiber are bounded, the T-matrix shows that the misalignment not only causes the loss of power at the connection interface, but it also leads to the creation of unbound rays and leaky rays in the second fiber. This is due to the fact that some of the rays enter the second fiber cross section where the local numerical aperture is smaller than

0.28 0.14 0.06 0.04 0.03 0.01 0.00 0.00 0.00 0.00 0.00 0.00

0.11 0.19 0.13 0.07 0.06 0.05 0.03 0.01 0.00 0.00 0.00 0.00

0.22 0.11 0.17 0.13 0.06 0.06 0.04 0.04 0.02 0.01 0.00 0.00

0.22 0.11 0.11 0.13 0.12 0.05 0.07 0.05 0.04 0.03 0.02 0.00

0.17 0.17 0.07 0.11 0.10 0.12 0.06 0.06 0.06 0.04 0.03 0.03

0.00 0.14 0.15 0.06 0.11 0.08 0.10 0.06 0.06 0.05 0.05 0.03

0.00 0.14 0.13 0.14 0.04 0.11 0.07 0.09 0.07 0.05 0.05 0.06

0.00 0.00 0.13 0.10 0.13 0.04 0.11 0.06 0.08 0.07 0.06 0.04

0.00 0.00 0.06 0.13 0.08 0.13 0.03 0.11 0.06 0.07 0.07 0.06

0.00 0.00 0.00 0.07 0.12 0.06 0.13 0.03 0.11 0.06 0.07 0.06

0.00 0.00 0.00 0.04 0.08 0.12 0.06 0.13 0.02 0.10 0.07 0.06

0.00 0.00 0.00 0.00 0.06 0.06 0.12 0.05 0.12 0.02 0.09 0.07

0.00 0.00 0.00 0.00 0.01 0.06 0.06 0.10 0.04 0.12 0.02 0.08

0.00 0.00 0.00 0.00 0.00 0.04 0.07 0.06 0.09 0.04 0.12 0.02

0.00 0.00 0.00 0.00 0.00 0.00 0.03 0.06 0.07 0.08 0.04 0.11

0.00 0.00 0.00 0.00 0.00 0.00 0.02 0.04 0.06 0.07 0.08 0.04

0.00 0.00 0.00 0.00 0.00 0.00 0.00 0.03 0.05 0.05 0.08 0.07

0.00 0.00 0.00 0.00 0.00 0.00 0.00 0.01 0.03 0.06 0.05 0.07

0.00 0.00 0.00 0.00 0.00 0.00 0.00 0.00 0.02 0.03 0.05 0.05

0.00 0.00 0.00 0.00 0.00 0.00 0.00 0.00 0.00 0.04 0.04 0.05

0.00 0.00 0.00 0.00 0.00 0.00 0.00 0.00 0.00 0.00 0.05 0.04

0.00 0.00 0.00 0.00 0.00 0.00 0.00 0.00 0.00 0.00 0.01 0.04

0.00 0.00 0.00 0.00 0.00 0.00 0.00 0.00 0.00 0.00 0.00 0.02

TL = 1.339 dB

Fig.3.2 A typical T matrix for lateral mismatch of 10μm

the local numerical aperture of the first fiber where the rays emanated from. Hence, these rays will not be bound and will radiate outside the second fiber. Those rays which enter the second fiber with position and orientation as such that their mode group number $m > M$, belong to leaky mode groups which will subsequently lead to the tunneling of optical power from the fiber core. A characteristic plot of the loss with respect to the lateral offset of the two fibers is given in Fig.3.3 parameterized by the ratio of the radii of the second fiber to the first fiber. The results are compared with those obtained in reference [1]. A plot of the transmission with respect to the lateral offset is given in Fig.3.4. The curve of transmission versus the lateral offset obtained by C.M.Miller is also provided in this figure and is represented by filled circles.

II.*Two fibers with axial separation*: This is another special case where the end surfaces of the two fibers are separated by a distance of D_3 from each other. A characteristic plot of the loss with respect to the separation distance is given in Fig 3.6. This figure shows zero loss up to a short distance. This feature is due to the fact that the ray distribution (introduced in Chapter 2) emanating from the first fiber does not include the edges of the crossectional surface. Thus, the rays leaving the first fiber at angles within the limit of the numerical aperture of the fiber may travel a short distance between the two fibers and still land on the crossection of the second fiber. Hence, there will be no loss for a short separation distance between the two fibers. The fluctuation of this curve indicates the discrete nature of the loss mechanism associated with the loss of individual groups of rays.

III.*Two fibers with angular mismatch*: This special case focuses on

the performance of two fibers with angular misalignment of α without axial separation. A characteristic plot of the loss with respect to α is given in Fig. 3.7 parameterized by the transmission coefficient between the two fibers.

A comparison of Figs 3.3 and 3.6 reveals an interesting feature of connectors. These figures indicate that the curves of loss with respect to lateral offset and angular misalignment is identical. This feature can be explained by recalling the procedure for mode excitation. Consider Eq. (2.14), by introducing normalized spatial coordinate $\rho = r/a$ and angular coordinate $\xi = k_{\perp}/k_{\perp m}$ Eq. (2.14) can be written as [3]

$$\frac{m}{M} = \rho^2 + \xi^2 \qquad (3.13)$$

The fact that ρ and ξ are interchangeable in this equation implies that the phase-space volume occupied by the excited mode groups in a graded index fiber exhibits a rotational symmetry.

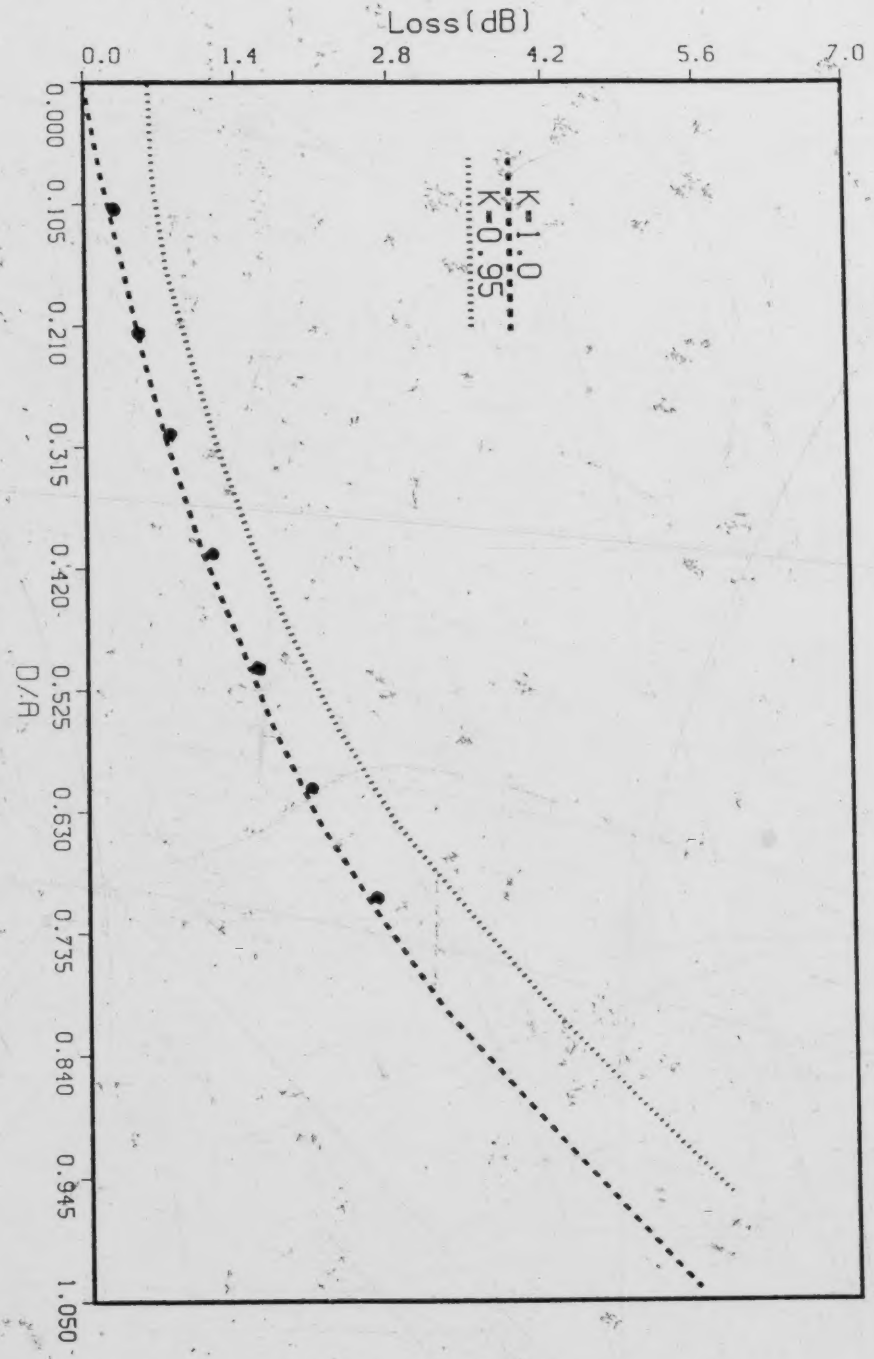

Fig.3.3 Plot of loss versus lateral offset parameterized by the ratio of the radii of the second fiber to the first fiber.

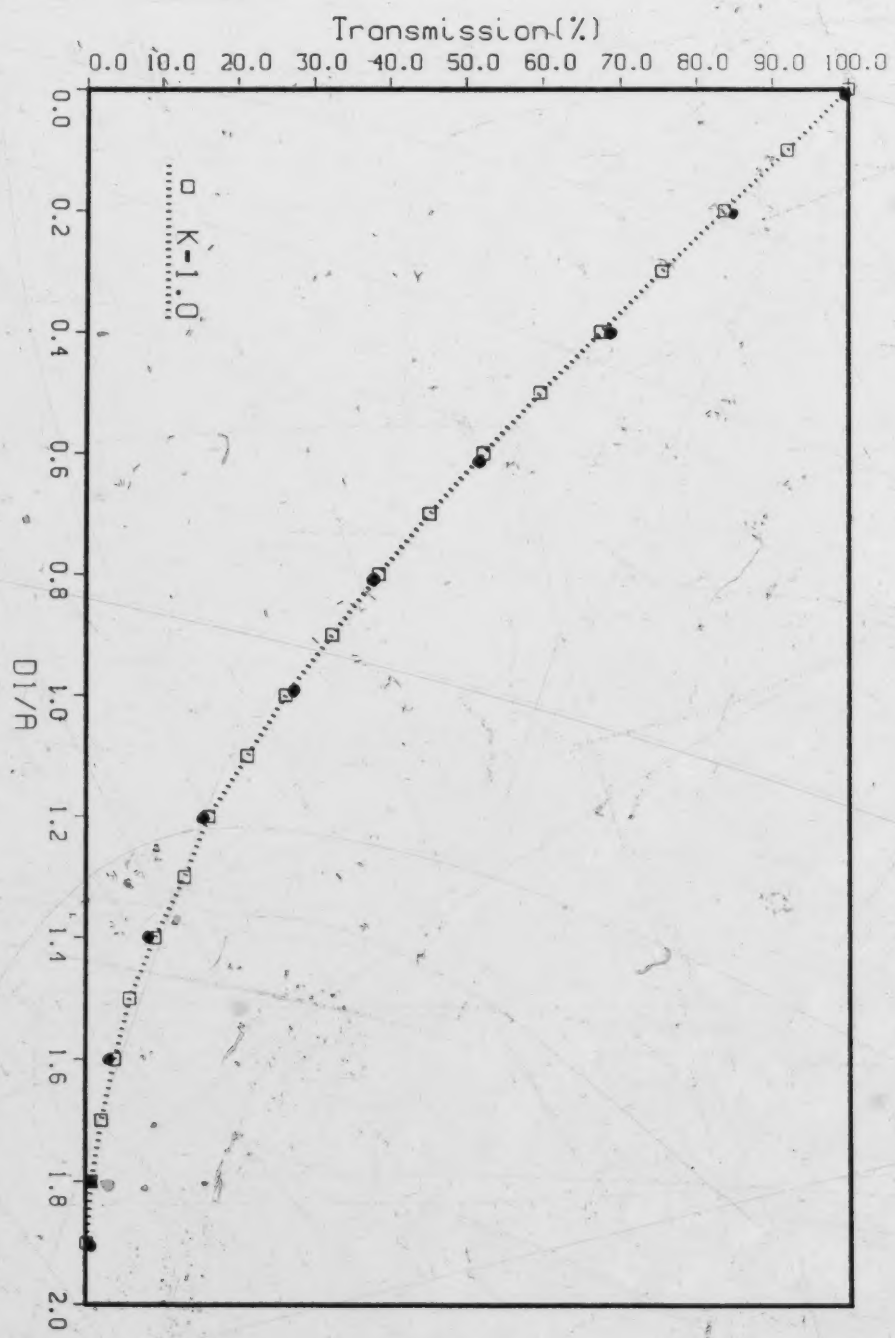

Fig.3.4 Plot of transmission versus lateral offset.

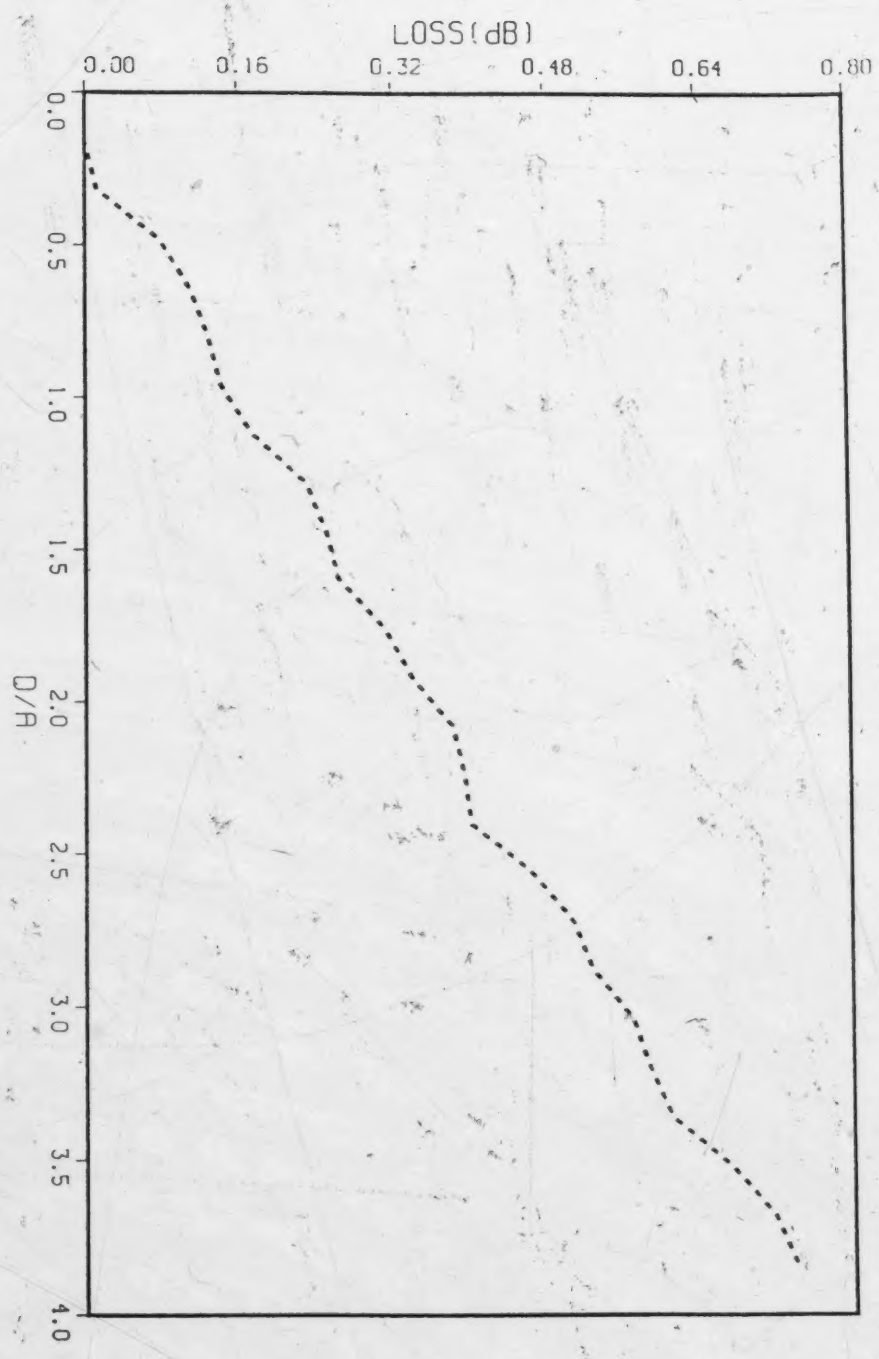

Fig.3.5 Plot of loss versus axial separation.

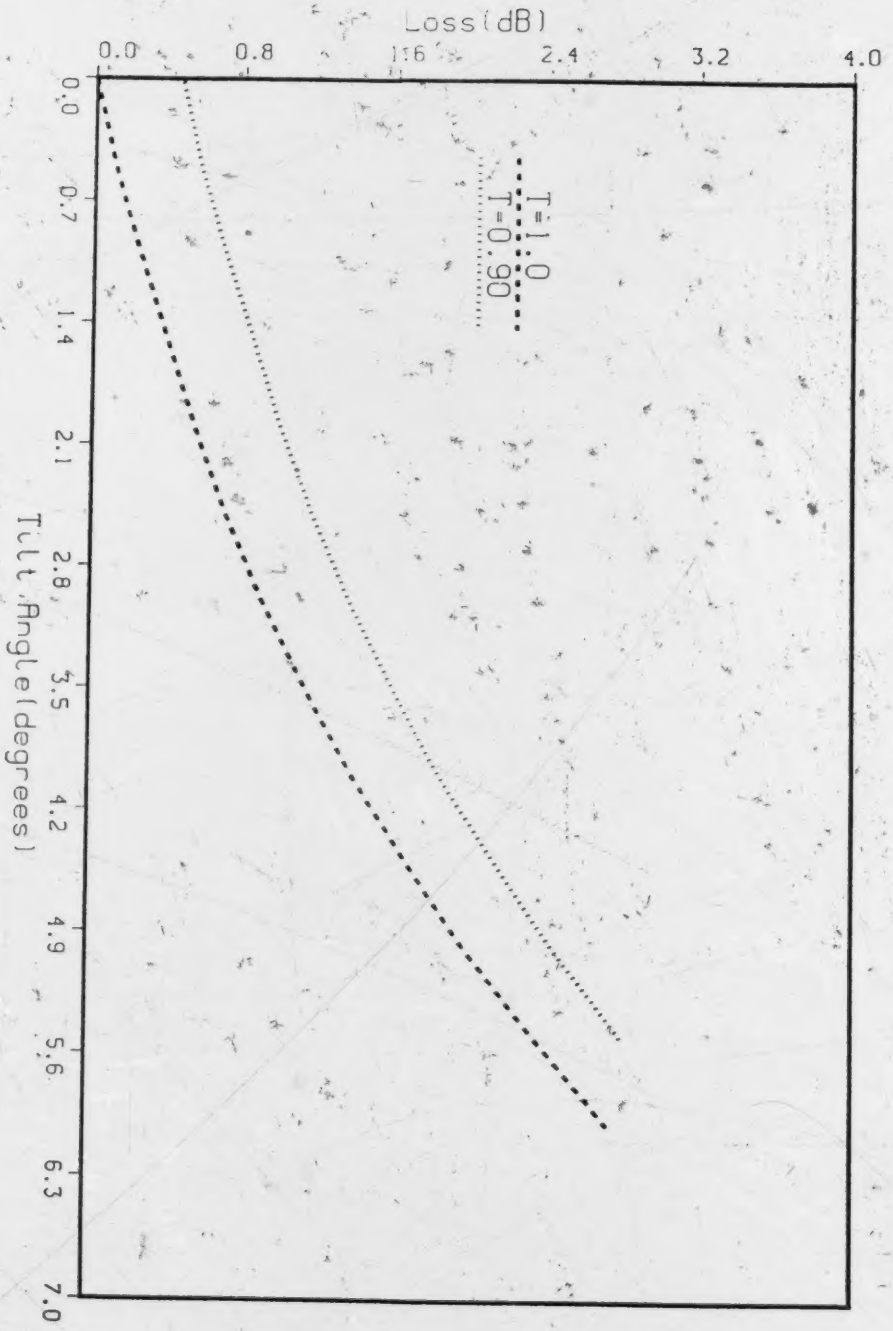

Fig.3.6 Plot of loss versus angular misalignment parameterized by the transmission coefficient between the two fibers

CHAPTER 4

BENT FIBER TAP

4.1 RAY EQUATIONS

It is well known that any geometrical deformation of an optical fiber leads to the coupling of power among modes. The coupling of power from guided modes to radiation modes leads to the loss of optical power from the fiber core [11]. There are several methods of calculating the loss from guided modes of a circularly bent fiber [42-49]. An alternative approach which is developed in Reference [8] is reviewed in this chapter . The analysis of circularly bent fibers requires the solution of the ray equations in a rotating coordinate system with respect to a stationary frame of reference. A circularly bent fiber in the y-z plane of a stationary coordinate system with a radius of curvature R is shown in Fig.4.1. The origin of the rotating coordinate system (X, Y, Z) is positioned on the fiber axis from which the position of the ray is determined.

Given the index of refraction as in Eq.(2.6) and the above-mentioned geometry, the equations of motion for a ray can be determined using the procedure introduced in Section (2.2). However, the effect of curvature can be introduced by the following choice of the position and the orientation coordinates of the ray [8].

$$\bar{X} = X\,\hat{x} + (R + Y)\,\hat{r} \tag{4.1}$$

$$\bar{k} = k_x\hat{x} + k_y\hat{y} + k_z\hat{z} \tag{4.2}$$

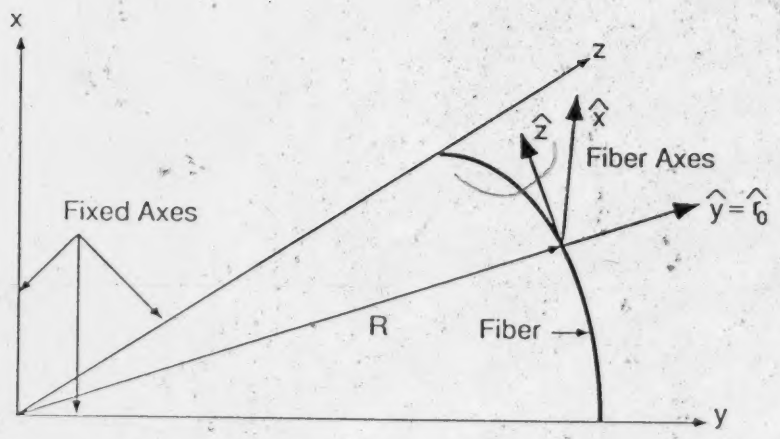

Fig.4.1 Schematic diagram of a circularly bent fiber with radius of curvature R and the rotating coordinate axis Y Z.

Where $\hat{x}$, $\hat{y}$, $\hat{z}$, and $\hat{r}$ are the unit vectors in X, Y, Z and radial directions respectively and R is the radius of curvature of the fiber. After a number of steps the equations of motion can now be written as [8]

$$\frac{d^2X}{d\tau^2} + Q^2V^2X = 0 \tag{4.3}$$

$$\frac{d^2Y}{d\tau^2} + Q^2V^2Y = \frac{V^2k_{zo}^2\left(R + Y_o\right)^2}{\omega^2\left(R + Y\right)^3} \tag{4.4}$$

$$\frac{dZ}{d\tau} = (C_o^2/\omega)\, k_z \tag{4.5}$$

where $V=C_o/n_1$, Y_o is the initial y-coordinate of the ray and Z is the distance along the fiber axis. From Eq.(4.5) a relation between $Z(\tau)$ and τ is found

$$Z(\tau) = Z_o + (C_o^2/\omega)\, k_z \tau \tag{4.6}$$

where k_z for a bent fiber is a function of Y as follows

$$k_z = \frac{k_{zo}\left(R + Y_o\right)}{\left(R + Y\right)} \tag{4.7}$$

Assuming that $R >> Y_o$ and expanding the term $1/(R + Y)$ and retaining the first term in the expansion gives

$$k = k_{zo} \tag{4.8}$$

Using Eq.(4.8) and the relation $d\tau = dt/n_1^2$ leads to further simplifications of Eqs.4.3 assuming that $Z_o=0$.

$$\frac{d^2X}{d\tau^2} + Q_1^2 X = 0 \qquad (4.9)$$

where $Q_1 = \frac{Q}{(1 + 2\Delta\, m_1/M)^{1/2}}$ and m_1 is the mode group number to which the ray belongs at the input. Furthermore, a Taylor expansion of the right hand side of Eq.(4.4) around Y=0 up to the first term and using the assumption of $R >> Y_o$, Eq.(4.4) can be written as

$$\frac{d^2Y}{d\tau^2} + Q_1^2 Y = \frac{1}{R} \qquad (4.10)$$

The solutions of Eq.(4.9) and (4.10) are as follows

$$X(Z)=X_o \cos(Q_1 Z) + (k_{xo}/n_1 k_o Q) \sin(Q_1 Z) \qquad (4.11)$$

$$Y(Z)=(Y_o - \frac{1}{Q_1^2 R})\cos(Q_1 Z) + (k_{yo}/n_1 k_o Q) \sin(Q_1 Z) + \frac{1}{Q_1^2 R} \qquad (4.12)$$

A comparison of Eq.(4.11) and (4.12) with those derived in Reference [50] shows a perfect agreement within the limit of paraxial approximation where $Q_1 = Q$. Having found X(Z) and Y(Z), the orientation of the ray is determined to be

$$k_x(Z) = k_{xo}\cos(Q_1 Z) - X_o n_1 k_o Q \sin(Q_1 Z) \qquad (4.13)$$

$$k_y(Z) = k_{yo}\cos(Q_1 Z) - n_1 k_1 Q\left(Y_o - \frac{1}{Q_1^2 R}\right)\sin(Q_1 Z) \qquad (4.14)$$

Eqs. (4.11) through (4.14) describe the trajectory of a ray traveling inside a circularly bent fiber. A comparison of Eq. (4.11) through (4.14) with those of (2.27) and (4.30) reveals an interesting feature of the circularly bent fibers. The comparison indicates a shift in the position of the rays in the direction of the bend by an amount $1/Q_1^2R$. This shift depends on the mode group number m. Rays belonging to lower order mode groups experience larger shifts than those belonging to higher order mode groups. Also, the shift depends on the radius of curvature of the bend. The larger the radius of curvature the smaller the shift will be. If the radius of curvature approaches infinity (which is the case for a straight fiber) the shift in the position of the rays will vanish and the solution is the same as in straight fiber. A schematic diagram of this feature is presented in Fig. 4.2. This figure indicates that the motion of the rays in X-Y plane is elliptical with the center of the ellipse shifted by $1/(Q_1^2R)$. For a conventional fiber with NA/a = 0.2/25, on-axis refractive index n_1=1.46 and a radius of curvature R=5mm the shift in the position of the axis will be 13.32μm which is approximately half the fiber core radius. This shift may cause a ray to leave the core and thus induce a loss.

4.2 LOSS MECHANISMS IN A BENT FIBER

Owing to the curvature of the fiber, all the rays inside the fiber core will eventually be lost by one of the two loss mechanisms, namely, refraction and tunneling[50]. Refraction refers to the loss incurred when a ray leaves the fiber's core. Tunneling refers to the gradual loss

of power from the fiber core as the rays advance along the fiber. A ray with a periodic trajectory loses a fraction of its power at each maximum distance from the fiber axis in the direction of the bend. The term tunneling is borrowed from quantum mechanics and means that for a particle inside a potential well there is a finite probability of finding this particle outside the potential well if there is a lower potential region to tunnel to [19,20]. The probability of a particle tunneling from one side of the potential well may be increased by altering the shape of the potential well. This is precisely what happens to the rays (photon trajectories) in a bent fiber where the centrifugal force due to the curvature creates a pseudo potential which plays the role of an altered potential well. Thus, the rays lose part of their power as they reach maxima along their trajectory in the direction of the bend as indicated in figure 4.2.

The total loss (the combined loss due to refraction and tunneling) at any point along the bent fiber can be determined from storing all the rays inside the fiber in the T-matrix which was introduced in Chapter 2. The incorporation of tunneling rays in the T-matrix requires a thorough investigation of the ray trajectory along the bent fiber.

4.2.1 A METHOD FOR CALCULATING THE LOSS

The procedure for the computation of loss can be best described by considering one ray carrying a fixed amount of power as an example and tracing it along the bent fiber. The position and the orientation of the ray entering the bent section of the fiber are in the discrete set introduced in Chapter 2. This in turn enables us to determine the mode group number m1 to which the ray initially belongs and the initial

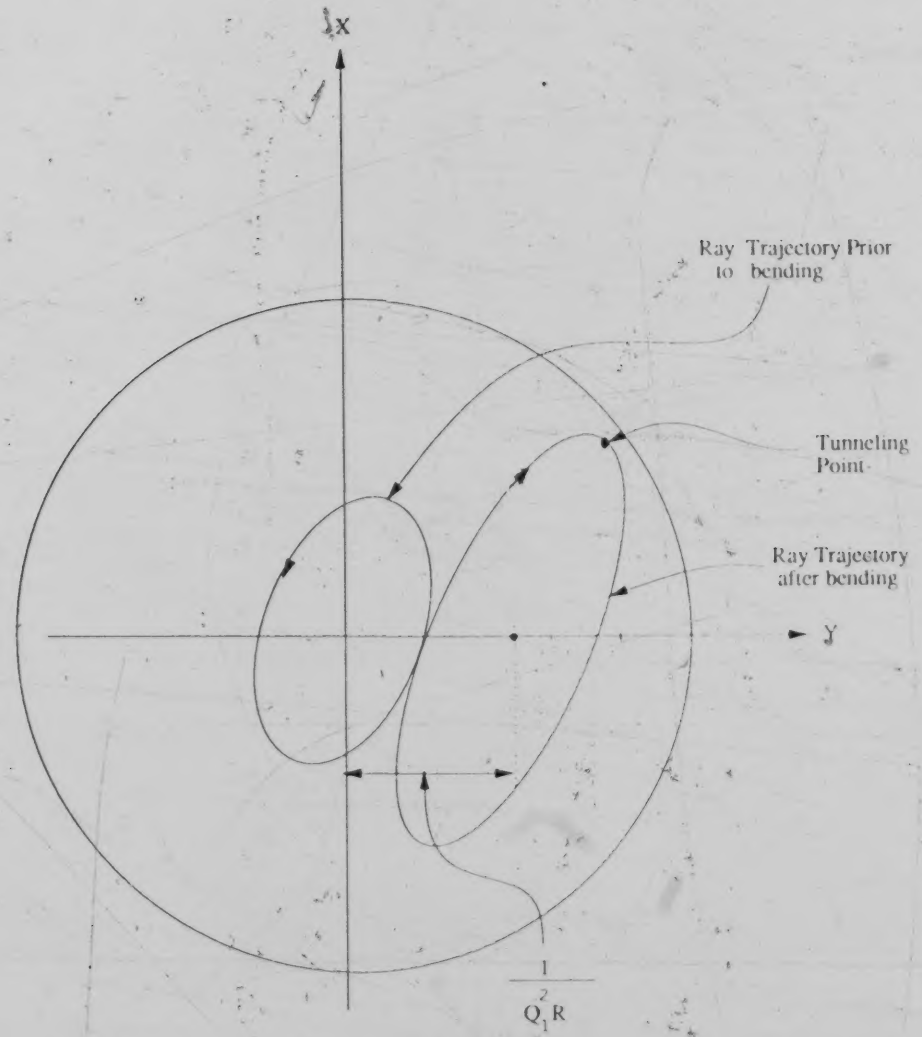

Fig.4.2 Projection of the ray path onto the X Y plane.

position and orientation of the ray with respect to the fiber axis. The ray, with its unique trajectory determined by Eq. (4.11) through (4.14), is then traced along the bent fiber by incrementing the distance along the bend by differential amounts of ΔZ. At each ΔZ the position X and Y and the orientation k_x and k_y of the ray is determined. The position of the ray at its maximum distance from the fiber core is then compared with the radius of the fiber core a. If the ray position $(r=(X + Y)^{1/2})$ is greater than the core radius a, the ray is considered lost. But if the maximum ray position in the direction of the bend is smaller than the core radius, the ray will lose a fraction of its power by tunneling. The amount of tunneling loss can be calculated from the expression for the tunneling probability given below [50]

$$T = \exp\left[-2/3\ k_o n_1 \rho_c \theta_g \left\{ \theta_g - 2\ D/\rho_c \right\}^{1/2} \right] \qquad (4.15)$$

where $\theta_g = \sin^{-1}\left[1 - (n_2/n_c)^2\right]^{1/2}$, n_c is the refractive index at the point where the ray reaches its maximum distance from the fiber core in the direction of the bend, n_2 is the cladding index of refraction and $\rho_c = \rho_1\rho_2/(\rho_1\cos^2\theta + \rho_2\sin^2\theta)$ with $\rho_1 = r_{max}$ and $\rho_2 = r_{max} + R/\cos\phi$ $(\phi = Y/(Y_{max}^2 + X_{max}^2)^{1/2})$ being the principal radii of curvature in the direction of the bend with constant surface of refractive index n_c and θ is the angle between the ray and the fiber axis. Since the trajectory of the ray is periodic, the ray loses the same amount of power at each peak. Hence, until the ray reaches the point at which the T-matrix is to be determined, the ray will have lost a fraction of its power. An example of two tunneling rays is given in the tables below for a bend radius of R=8mm. The first column shows the location of the point along

the bend at which tunneling takes place. The second column gives the ray position r with respect to the fiber axis, the third column gives the ray's radial orientation k_r, the fourth column represents the loss due to tunneling and the last column represents the power remaining in the ray after each tunneling process. The ray is traced for a distance of five ray periods. These tables show that when the ray reaches its peak, the radial orientation vanishes, $k_r \simeq 0$, and the distance between successive tunneling points is one ray period. A comparison of Table.4.1a with Table.4.1b reveals that the amount of power loss due to tunneling is not the same for all the rays. To determine the T-matrix, at the point of observation the ray is assigned to a certain mode group m2 and added to a particular element of an m2 x m1 matrix. This procedure is applied to all the rays and stored in the respective elements of the matrix. Finally the T-matrix is obtained by dividing each element of the m2 x m1 matrix by the corresponding number of rays in the m1 mode group. A typical T-matrix at a distance of three ray period along the bend with bend radius R=5mm is given in Fig.4.3. The number at the bottom of the T-matrix is the total loss (the combined loss due to refraction and tunneling). A characteristic plot of total loss versus distance along the bend, parameterized by the radius of curvature of the bend is given in Fig.4.4 which compares well with the results obtained in reference [50] shown by filled circles. A comparison of Fig.4.4 with Fig.4.5 show that the amount of radiation and tunnelling losses differ between two fibers with different parameters and wavelengths. These figures show almost no loss up to a short distance from the beginning of the bend followed by a rapid loss of power up to a point and subsequently an exponential-like attenuation. This point corresponds to a distance of

Distance along fiber	ray position	ray orientation	tunneling loss	power remaining
525.00	24.31	0.06187	0.00853	0.99147
1650.00	24.31	0.05697	0.00867	0.98287
2775.00	24.32	0.05206	0.00881	0.97421
3900.00	24.32	0.04713	0.00881	0.96563
5025.00	24.32	0.04221	0.00880	0.95713
6150.00	24.33	0.03727	0.00871	0.94880
7275.00	24.33	0.03233	0.00854	0.94070
8400.00	24.33	0.02739	0.00829	0.93290
9525.00	24.33	0.02243	0.00798	0.92546
10650.00	24.33	0.01747	0.00767	0.91835
11775.00	24.33	0.01250	0.00724	0.91171

Table 4.1a

Distance along fiber	ray position	ray orientation	tunneling loss	power remaining
550.00	23.72	0.02807	0.00005	0.99995
1675.00	23.72	0.02376	0.00004	0.99991
2800.00	23.72	0.01943	0.00004	0.99987
3925.00	23.72	0.01509	0.00004	0.99983
5050.00	23.72	0.01075	0.00003	0.99980
6175.00	23.72	0.00640	0.00003	0.99977
7300.00	23.72	0.00205	0.00003	0.99974
8450.00	23.61	0.09438	0.00004	0.99970
9575.00	23.62	0.09023	0.00005	0.99965
10700.00	23.63	0.08607	0.00005	0.99960
11825.00	23.64	0.08189	0.00005	0.99955

Table 4.1b

slightly less than one ray period along the bent fiber. This characteristic behavior is due to the fact that the ray trajectory is periodic and hence, a ray that is destined to leave the fiber core will do so before completing one period. The majority of the refracted rays leave the core at a distance of slightly less than one ray period along the fiber. Hence, the rapid loss of power is due to refraction. Beyond a distance of one ray period the loss of power is solely due to tunnelling.

0.049 0.043 0.016 0.006 0.000 0.000 0.000 0.000 0.000 0.000 0.000 0.000
0.148 0.105 0.082 0.062 0.030 0.008 0.000 0.000 0.000 0.000 0.000 0.000
0.247 0.142 0.115 0.083 0.067 0.049 0.026 0.006 0.000 0.000 0.000 0.000
0.272 0.185 0.132 0.108 0.081 0.078 0.063 0.040 0.016 0.001 0.000 0.000
0.173 0.179 0.136 0.114 0.106 0.080 0.058 0.044 0.036 0.022 0.000 0.000
0.099 0.154 0.148 0.127 0.106 0.086 0.071 0.062 0.048 0.031 0.016 0.000
0.012 0.123 0.140 0.111 0.096 0.093 0.085 0.076 0.049 0.043 0.028 0.007
0.000 0.068 0.103 0.111 0.104 0.093 0.079 0.069 0.061 0.052 0.031 0.016
0.000 0.000 0.091 0.098 0.084 0.084 0.076 0.074 0.067 0.056 0.056 0.033
0.000 0.000 0.029 0.066 0.072 0.080 0.066 0.069 0.068 0.054 0.052 0.034
0.000 0.000 0.000 0.025 0.046 0.054 0.069 0.059 0.062 0.059 0.047 0.040
0.000 0.000 0.000 0.000 0.017 0.039 0.042 0.053 0.048 0.051 0.055 0.039
0.000 0.000 0.000 0.000 0.000 0.004 0.012 0.022 0.030 0.032 0.037 0.036
0.000 0.000 0.000 0.000 0.000 0.000 0.000 0.008 0.011 0.011 0.020 0.020
0.000 0.000 0.000 0.000 0.000 0.000 0.000 0.000 0.003 0.009 0.003 0.009
0.000 0.000 0.000 0.000 0.000 0.000 0.000 0.000 0.000 0.000 0.006 0.005
0.000 0.000 0.000 0.000 0.000 0.000 0.000 0.000 0.000 0.000 0.000 0.002
TL= 2.668 dB

Fig.4.3 A typical T-matrix at a distance of three ray periods along the bend.

As mentioned earlier the amount of loss depends on the radius of curvature of the fiber. This characteristic behavior is depicted in Fig. 4.6 for a fiber with a = 25μm, NA = 0.2 and λ = 1.3μm.

One desirable property of the bent fiber is its applicability for the purpose of eliminating undesirable modes from the fiber. This property of a bent fiber can be verified by observing the variation of modal power distribution at a number of positions along the bend. A schematic diagram of the modal power distribution at 0.1 and 10mm along the bend is given in Fig. 4.7. This figure shows that higher order mode groups are gradually eliminated from the fiber as the rays advance along the fiber. Finally, at a sufficiently long distance along the bend, the distribution of power among mode groups attains a steady state and steadily decreases.

The DMA can be determined from the diagonal elements of the T-matrix. Two typical DMA curves are given in Fig. 4.8. The upper curve in this figure shows DMA at a distance of 0.1mm from the beginning of the bend and the lower curve shows DMA at a distance of 10mm from the beginning of the bend.

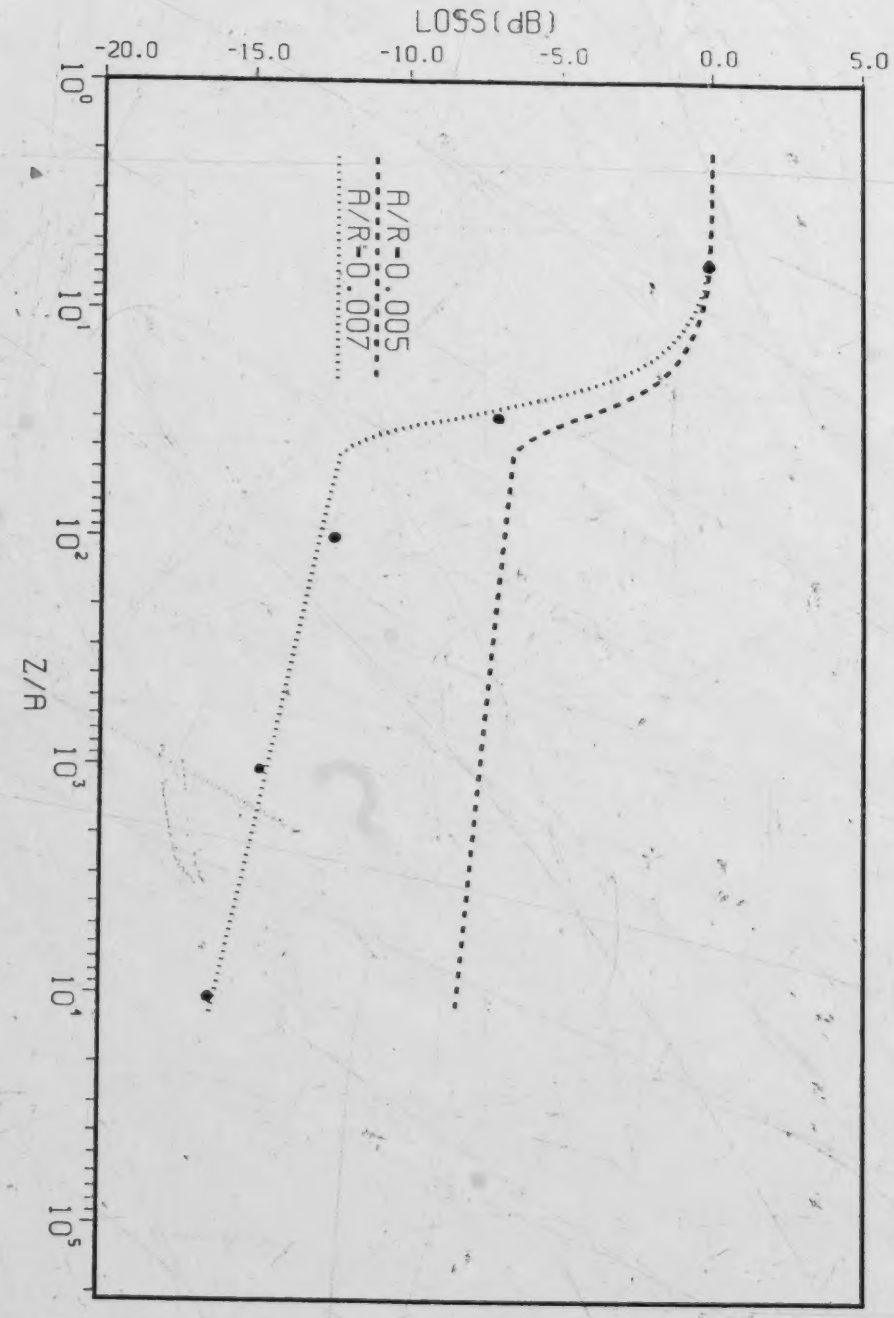

Fig.4.4 Plot of loss versus normalized distance along the bend parameterized by the radius of curvature of the bend for a fiber with A=50μm NA=0.159 and n_1=1.52

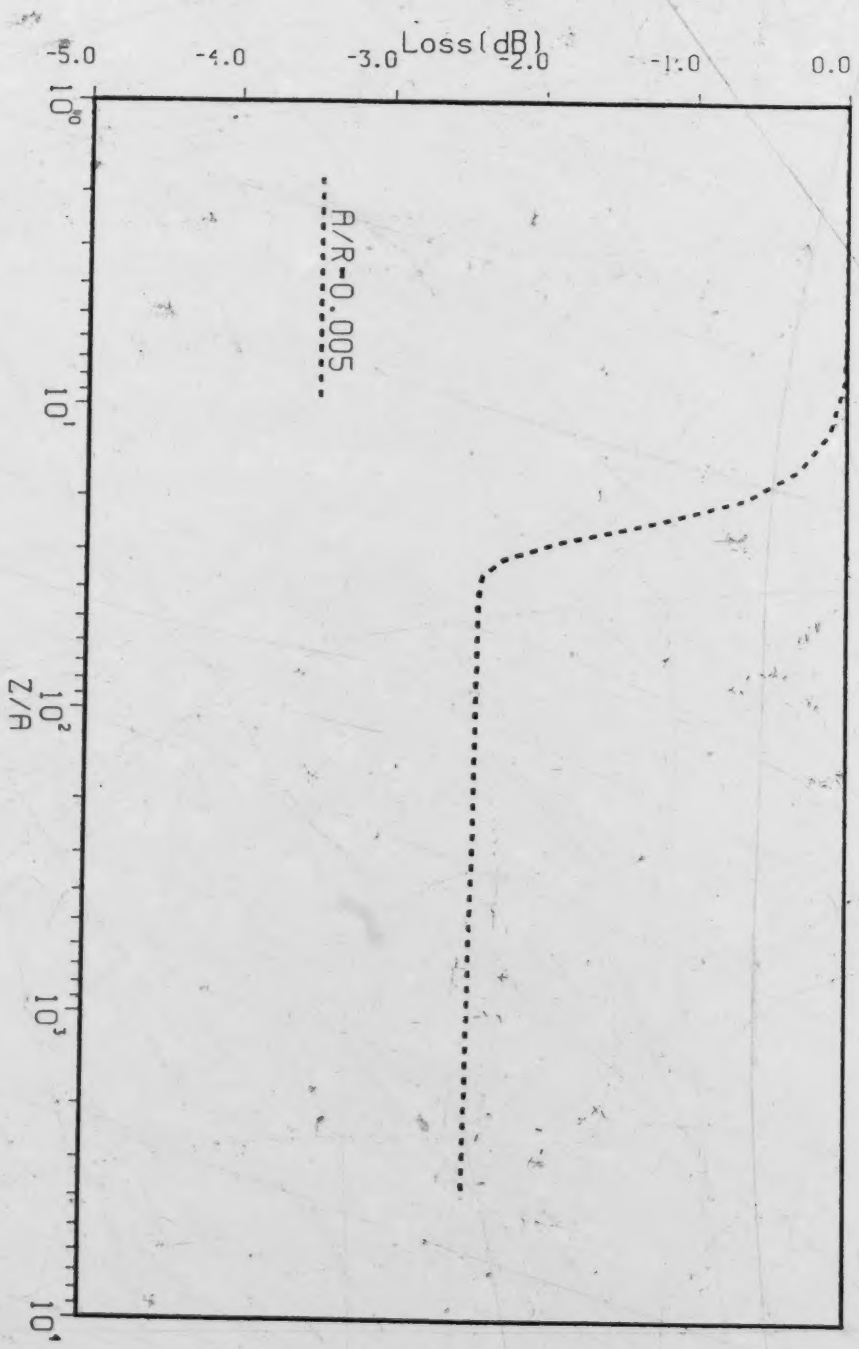

Fig.4.5 Plot of loss versus distance along the bend for a conventional fiber with A=25μm, NA=0.2 and n_1=1.46.

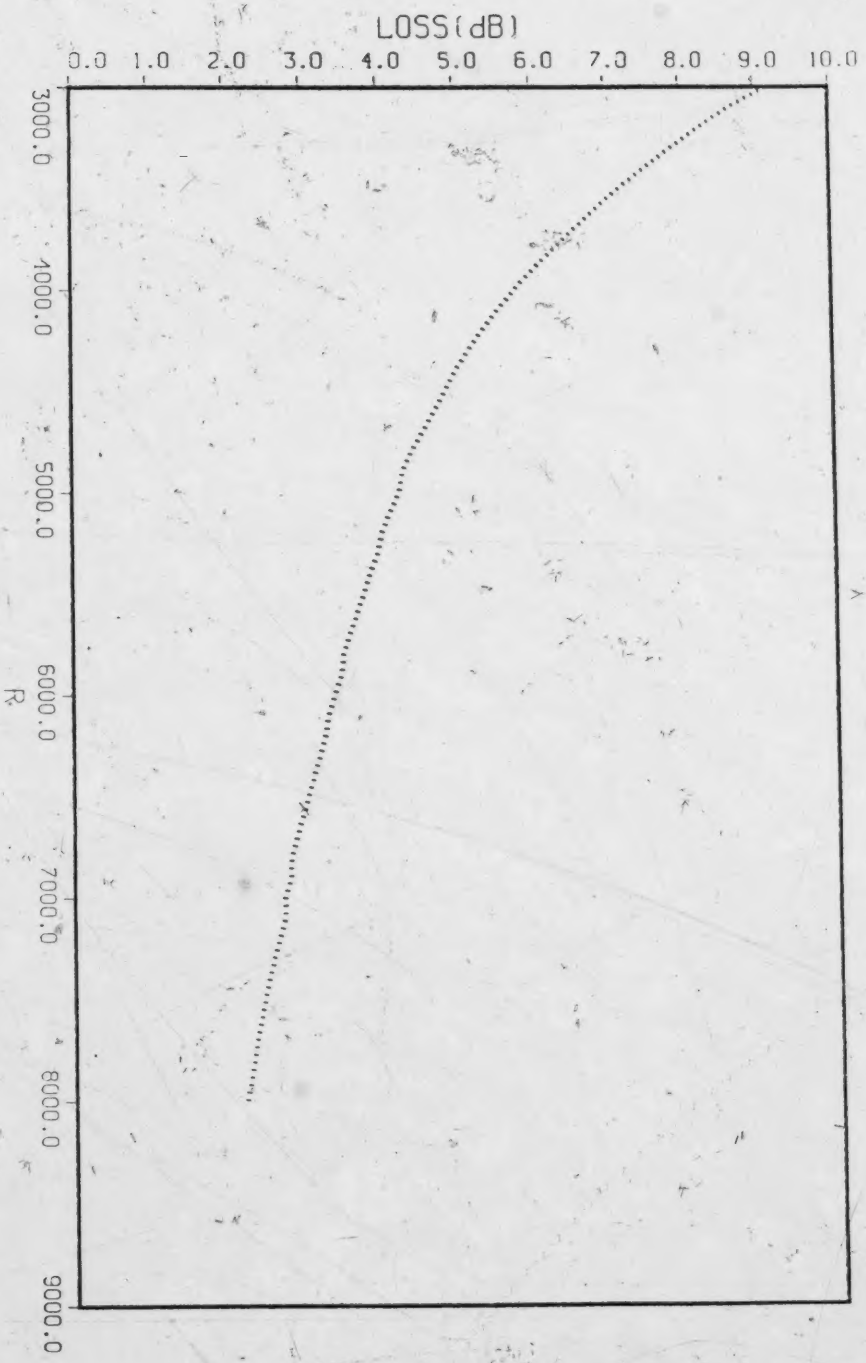

Fig.4.6 Atypical plot of loss versus the radius of curvature of the bend.

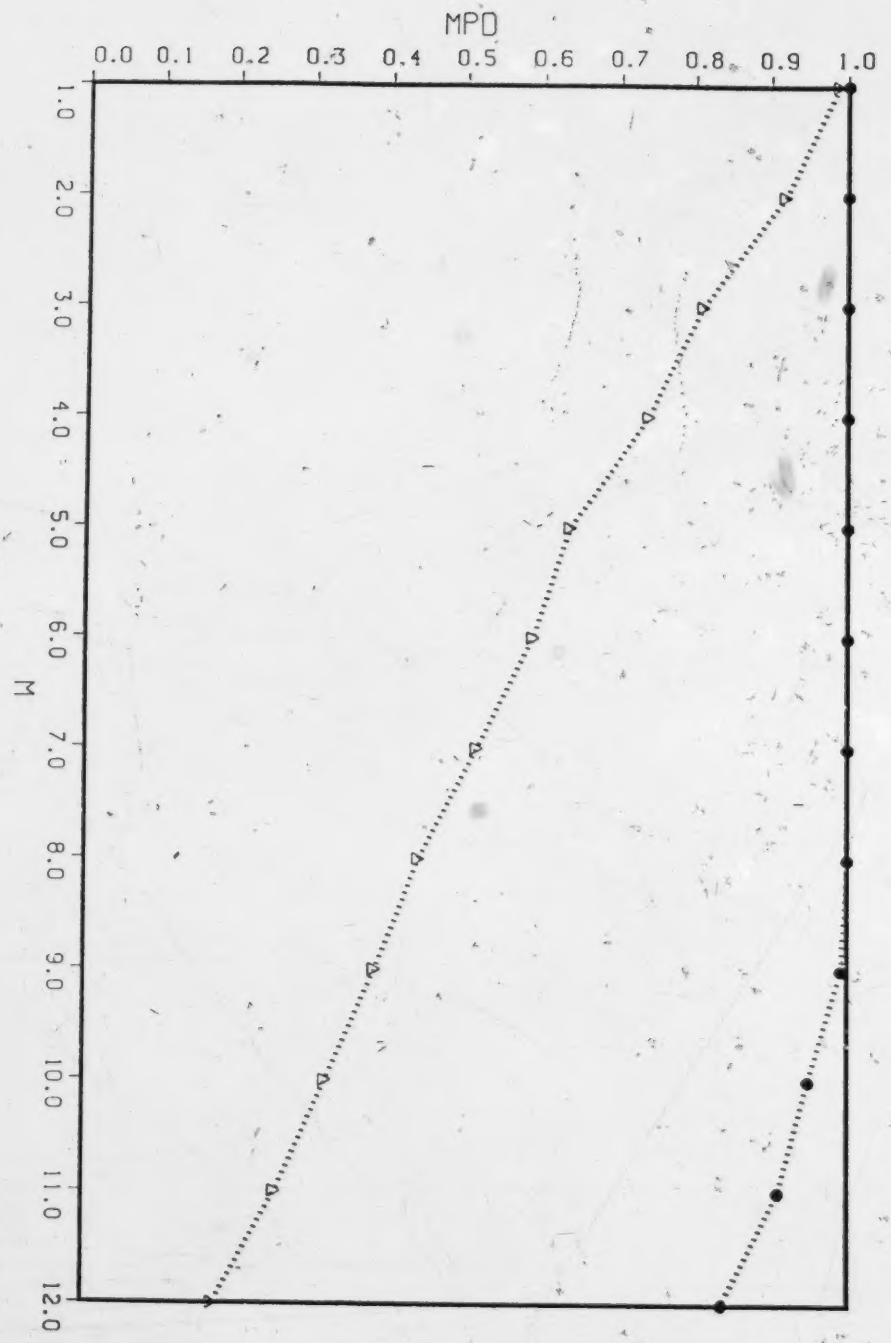

Fig.4.7 Plot of MPD at two different points along the bend

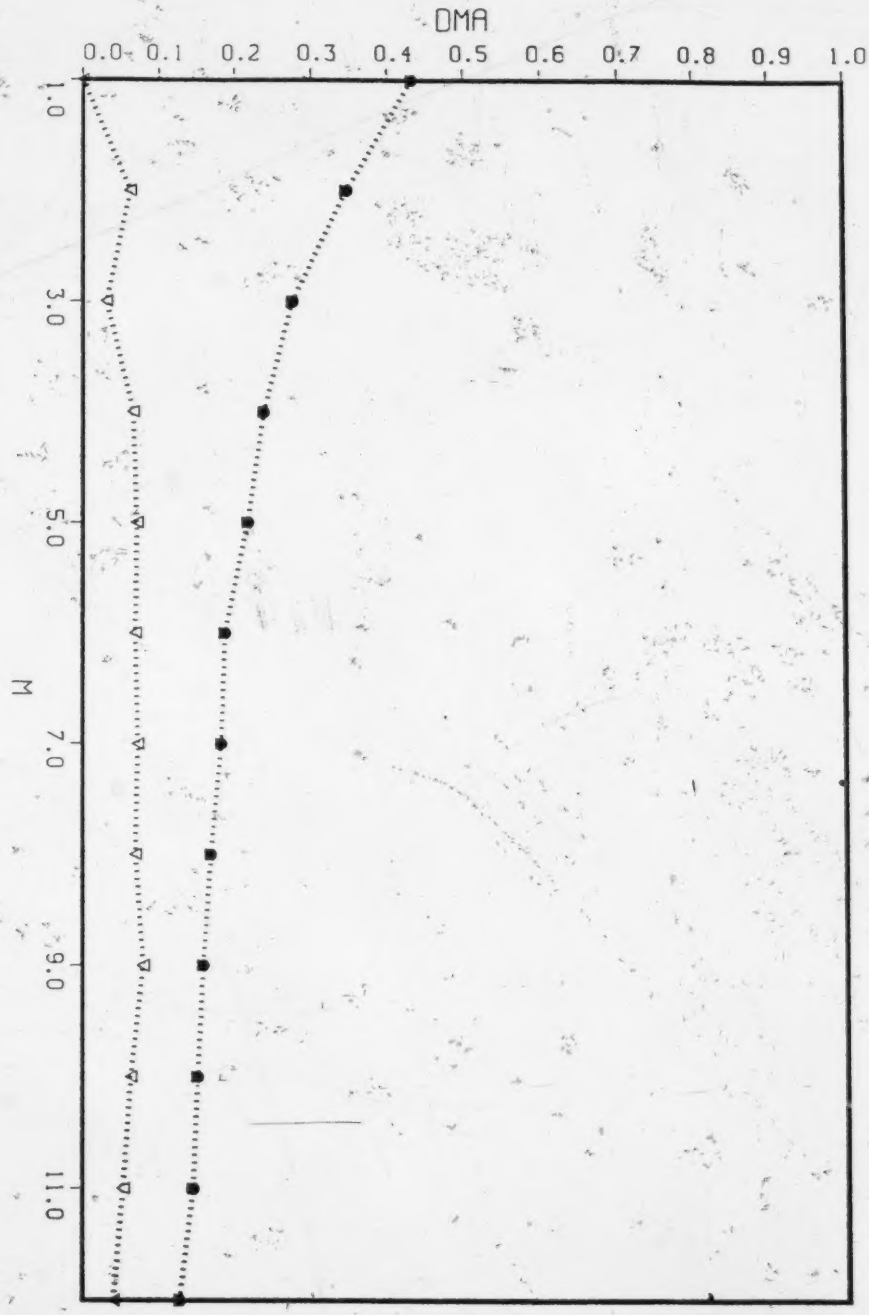

Fig.4.8 Plot of DMA at 0.1 and 10mm along the bend.

CHAPTER 5

MICROBENDING SENSORS

5.1 Ray Equations

This chapter is devoted to the analysis of graded index fiber with a finite length of periodic perturbations. This type of structure is commonly used as a sensor and is called a *microbending sensor*. A typical sensor is characterized by its amplitude, period and the number of periods in its total length. In practice this structure can be achieved by pressing a fiber between two plates with equally spaced grooves. This structure is shown in Fig 5.1. In this figure Λ and δ are the period and the amplitude of the sensor respectively, F is the force causing the deformation of the fiber axis and L is the total length of the deformation.

The first objective of this chapter is to analyze the performance of a single sensor subject to its parameter variation such as amplitude and period and the second objective is the study of serial sensors.

The analyses of sensors requires the solutions of the ray equations which describe the trajectory of a ray in the sensor. Referring to the derivation of ray equations in chapter 4, Eqs.(4.9) and (4.10) can be written as follows

$$\frac{d^2Y}{dZ^2} + Q_1^2 Y = \frac{1}{R(Z)} \qquad (5.1)$$

$$\frac{d^2X}{dZ^2} + Q_1^2 X = 0 \qquad (5.2)$$

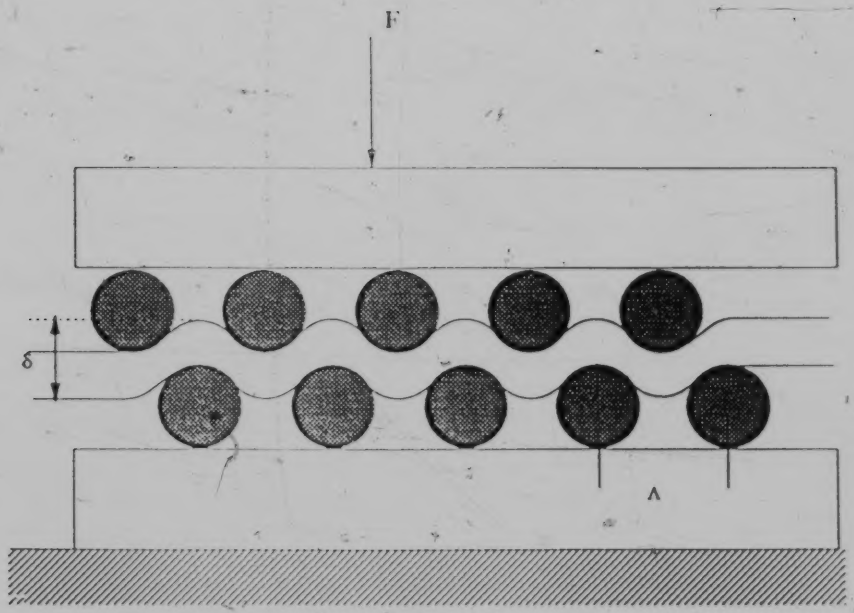

Fig.5.1 Schematic diagram of a microbending sensor with period Λ and amplitude δ.

where Q_1 is the same as in Chapter 4 and R(Z) is the periodic radius of curvature of the fiber. Assuming that the fiber has a periodic deformation in the Y direction, the position of the fiber axis can be expressed as follows [42].

$$Y1(Z) = \frac{\delta}{2} \cos\left(\frac{2\Pi}{\Lambda} Z\right) \tag{5.3}$$

Differentiating Eq. (5.3) twice with respect to Z gives the periodic curvature of the fiber [42].

$$\frac{1}{R(Z)} = - \frac{2\Pi^2}{\Lambda^2} \delta \cos\left(\frac{2\Pi}{\Lambda} Z\right) \tag{5.4}$$

The negative sign in Eq. (5.4) indicates the concaveness of the curvature in Y-Z plane. Substitution of Eq. (5.4) into Eq. (5.3) and assuming upward concaveness of the curvature gives

$$\frac{d^2Y}{dZ^2} + Q^2Y = (2\Pi^2/\Lambda^2)\, \delta \cos\left(\frac{2\Pi}{\Lambda} Z\right) \tag{5.5}$$

Eq. (5.5) and (5.2) are the equations of motion for a ray traveling along the sensor. The solutions to the above equations of motion describe the trajectory of a ray in the fiber core. The solutions are given below.

$$X(Z) = X_o \cos(Q_1 Z) + (k_{xo}/n_1 k_o Q) \sin(Q_1 Z) \tag{5.6}$$

$$Y(Z) = Y_o \cos(Q_1 Z) + (k_{yo}/n_1 k_o Q) \sin(Q_1 Z) + \frac{\Gamma}{(Q_1^2 - W^2)} \left[\cos(WZ) - \cos(Q_1 Z)\right] \tag{5.7}$$

where $\Gamma = 2\Pi^2\delta/\Lambda^2$ and $W = 2\Pi/\Lambda$ .The directions k_x and k_y of the ray are found to be

$$k_x(Z)=k_{xo}\cos(Q_1Z) - n_1 k_o X_o Q \sin(Q_1Z) \tag{5.8}$$

$$k_y(Z)=k_{yo}\cos(Q_1Z)-n_1 k_o Y_o Q\sin(Q_1Z) + \frac{n_1 k_o Q\Gamma}{(Q_1^2 - W^2)}\left[\sin(Q_1Z)-(W/Q_1)\sin(WZ)\right] \tag{5.9}$$

Equations (5.6) through (5.9) show that rays belonging to different mode groups have different periods specified by $RP = 2\pi/Q_1$. For example, the difference between the periods of the rays belonging to the lowest mode group (mode group one) and those belonging to the highest mode group (mode group twelve) is $\Delta RP=10\mu m$ for the fiber under consideration.

Having found $X(Z)$, $Y(Z)$, $k_x(Z)$ and $k_y(Z)$, the position $r(Z)$ and orientation $k_\perp(Z)$ of a ray can be determined at any point along the sensor. This enables us to assign a ray to a certain mode group which in turn allows for the determination of the T-matrix at any point along the sensor.

5.2 LOSS MECHANISMS IN A SENSOR

As mentioned earlier geometrical perturbations of a fiber's core gives rise to mode coupling and consequently to the loss of power from the fiber core. As in the case of constant bend, there are two mechanisms responsible for the loss of power in a sensor: refraction and tunneling.

Refraction loss refers to the number of rays leaving the fiber

core. In a sensor, this loss mechanism dominates for a few periods along the sensor beyond which refraction does not occur. This length depends on the relative difference between the ray period and the sensor period. For example, if the sensor's period is $\Lambda=4/3$ RP (RP=ray period) then the ray will have exhausted all its chances for leaving the fiber core in three sensor periods. Hence, in a distance of 3Λ a ray will either leave the core or remain inside the core. However, if the sensor's period is not a rational multiple of the ray period the motion of the rays is not periodic and hard to predict. The number of those rays which leave the core constitute the loss of power only due to refraction.

The second mechanism responsible for the loss of power is tunneling [50]. Tunneling occurs when a ray reaches its maximum distance from the fiber axis *in the direction of the bend*. It should be noted that the fiber has a sinusoidal curvature, therefore a ray most probably tunnels when its maxima in the direction of the bend is near to the fiber's maximum because the tunneling loss formula predicts stronger loss for smaller R [50]. However, tunneling does not occur at fiber's inflection points where the radius of curvature of the fiber is infinite (straight fiber).

5.2.1 A METHOD FOR CALCULATING THE LOSS

The procedure for calculating the loss in a microbending sensor is the same as for the constant bend introduced in Chapter 4. The expression for the tunneling probability given in Chapter 4 can be used to determine the tunneling loss. However, in a sensor where the curvature of the fiber is a periodic function of Z, the radius of curvature ρ_c becomes a periodic function of Z through $\rho_2(z)$. A typical

example of the T-matrix at the distance of 7mm along the sensor with δ=10μm and Λ=1.5mm is given in Fig.5.2. The number of columns of the T-matrix represents the number of mode groups at the input and the number of rows represents the number of mode groups at the point of observation (at distance of 7mm). The fact that the number of rows of the T-matrix is larger than the number of columns signifies the presence of leaky modes which were created by the geometric deformation of the fiber. The number at the bottom of the T-matrix represents the total loss.

A characteristic plot of loss versus distance along the sensor parameterized by the sensor amplitude is depicted in Fig 5.3. This figure indicates a rapid loss due to refraction followed by an exponential-like attenuation which is solely attributed to tunneling. The periodicity in the curve of loss versus distance is indicative of the fact that losses occur predominantly at those points along the sensor where the radius of curvature of the fiber is the smallest. Fig.5.4 again shows the loss versus distance characteristics of the sensor for longer distance along the sensor.

5.3 CHARACTERISTICS OF MICROBENDING SENSORS

Microbending sensors exhibit a number of interesting features. There are numerous publications which focus on the theoretical and experimental verification of these features [11,51,52,53,54]. In this chapter the analysis of these features is carried out using geometrical optics. Those features which will be analyzed here are; (1) the modal power distribution obtained from the T-matrix, (2) variation of loss with respect to change in sensor amplitude, (3) variation of loss with

respect to change in sensor period and finally, (4) study of the performance of two serial sensors.

0.000	0.000	0.016	0.009	0.000	0.000	0.000	0.000	0.000	0.000	0.000	0.000
0.062	0.093	0.078	0.065	0.049	0.029	0.018	0.000	0.000	0.000	0.000	0.000
0.222	0.130	0.086	0.068	0.059	0.053	0.042	0.043	0.018	0.007	0.000	0.000
0.160	0.123	0.095	0.077	0.069	0.066	0.062	0.056	0.049	0.036	0.029	0.005
0.111	0.093	0.099	0.096	0.086	0.070	0.062	0.045	0.056	0.051	0.041	0.021
0.136	0.123	0.078	0.093	0.074	0.070	0.069	0.068	0.053	0.055	0.039	0.027
0.259	0.111	0.119	0.080	0.084	0.076	0.067	0.058	0.050	0.036	0.036	0.025
0.049	0.142	0.095	0.086	0.074	0.086	0.061	0.059	0.045	0.040	0.035	0.029
0.000	0.080	0.107	0.092	0.075	0.052	0.063	0.056	0.049	0.034	0.024	0.020
0.000	0.093	0.077	0.073	0.078	0.063	0.036	0.043	0.028	0.027	0.022	0.017
0.000	0.012	0.062	0.048	0.057	0.027	0.055	0.024	0.027	0.018	0.016	0.007
0.000	0.000	0.017	0.030	0.024	0.037	0.008	0.032	0.014	0.016	0.008	0.004
0.000	0.000	0.000	0.005	0.013	0.016	0.028	0.005	0.024	0.010	0.006	0.001
0.000	0.000	0.000	0.000	0.004	0.007	0.011	0.021	0.004	0.011	0.005	0.003
0.000	0.000	0.000	0.000	0.000	0.001	0.005	0.006	0.015	0.001	0.003	0.001
0.000	0.000	0.000	0.000	0.000	0.000	0.000	0.003	0.001	0.011	0.000	0.000
0.000	0.000	0.000	0.000	0.000	0.000	0.000	0.000	0.002	0.001	0.007	0.000
0.000	0.000	0.000	0.000	0.000	0.000	0.000	0.000	0.000	0.001	0.001	0.003
0.000	0.000	0.000	0.000	0.000	0.000	0.000	0.000	0.000	0.000	0.001	0.000
0.000	0.000	0.000	0.000	0.000	0.000	0.000	0.000	0.000	0.000	0.000	0.001

TL = 3.189 dB

Figure.5.2 A typical T-matrix at a distance of 7mm along the sensor

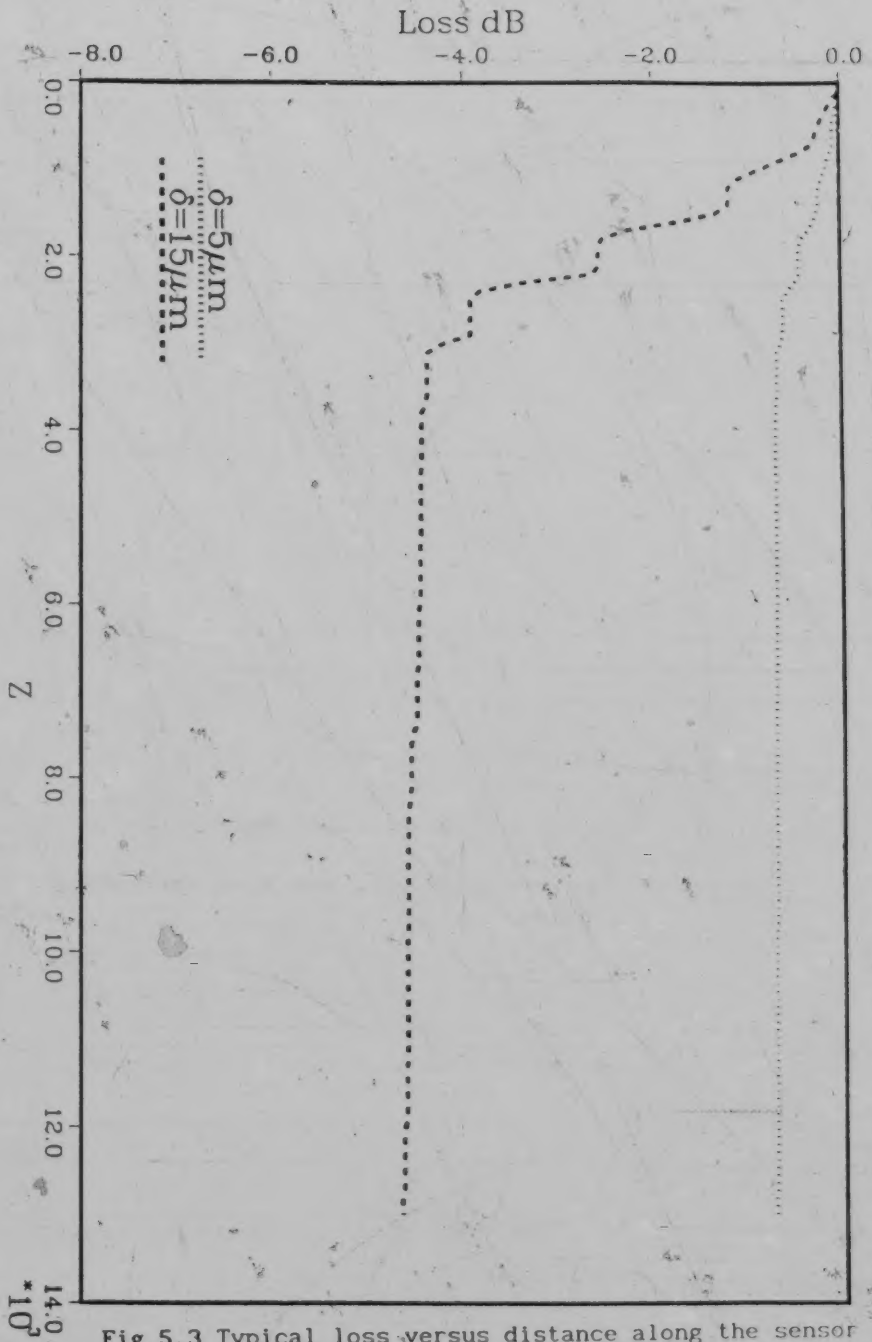

Fig. 5.3 Typical loss versus distance along the sensor parameterized by the amplitude of the sensor

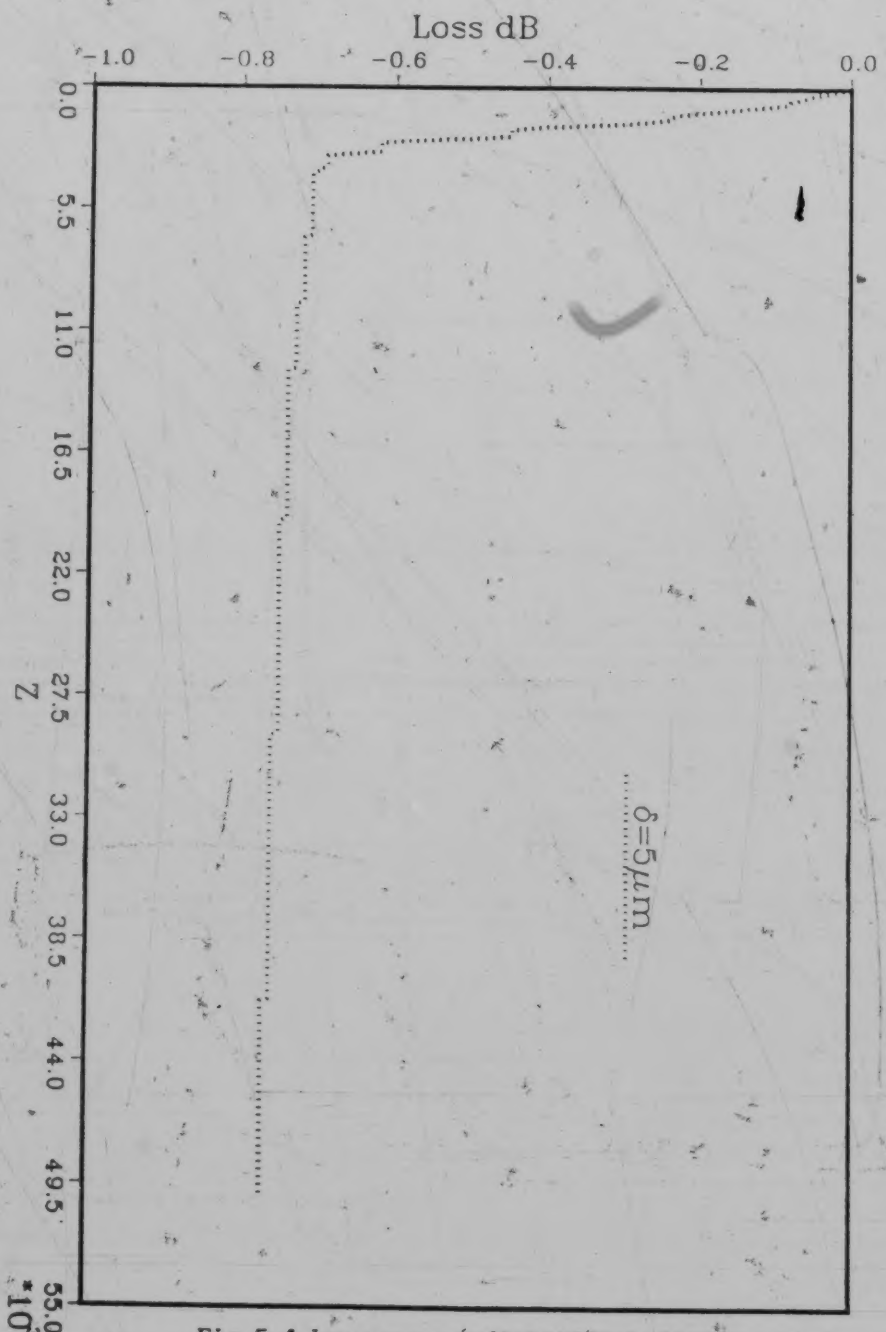

Fig.5.4 Loss versus distance along the sensor.

5.3.1 THE MODAL POWER DISTRIBUTION

The T-matrices at three different points along the sensor with fixed amplitude and period are determined and the modal power distribution at those points along the sensor is obtained from the above matrices. Fig.5.5 depicts the modal power distribution at distances of 0.1, 5.0 and 7.5mm along a sensor with amplitude δ=10μm and period Λ=1.5mm. Figure 5.5 further confirms the mode stripping property of the microbending sensors. The figure also shows that the distribution of power among mode groups at 5mm and 7.5mm along the sensor coincide with each other. Thus, the MPD in a sensor tends to reach steady state beyond a distance of 5mm along the sensor with parameters a=25μm, NA=0.2 and λ=1.3μm.

5.3.2 EFFECT OF CHANGE IN MICROBENDING AMPLITUDE ON POWER LOSS

The procedure for calculating this effect is as follows. A conventional fiber of NA=0.2 , a=25μm and on-axis refractive index n_1= 1.46 is used and the sensor period is set to a fixed value. Initially, the sensor amplitude is set to δ=0.4μm and rays with equal powers are launched into input of the sensor according to the procedure introduced in Chapter 2. Allowing the rays to travel a distance of 8mm along the sensor, which is sufficiently long for the rays to undergo refraction and tunneling losses, the power remaining in the fiber is determined at the output. This procedure is repeated many times and every time the amplitude is incremented by 0.4μm. The characteristic sensor behavior is depicted in Fig.5.6 parameterized by the period of the sensor. Fig.5.6 shows that the curve of loss versus sensor amplitude is approximately parabolic which agrees Ref. 51. We also see that the loss

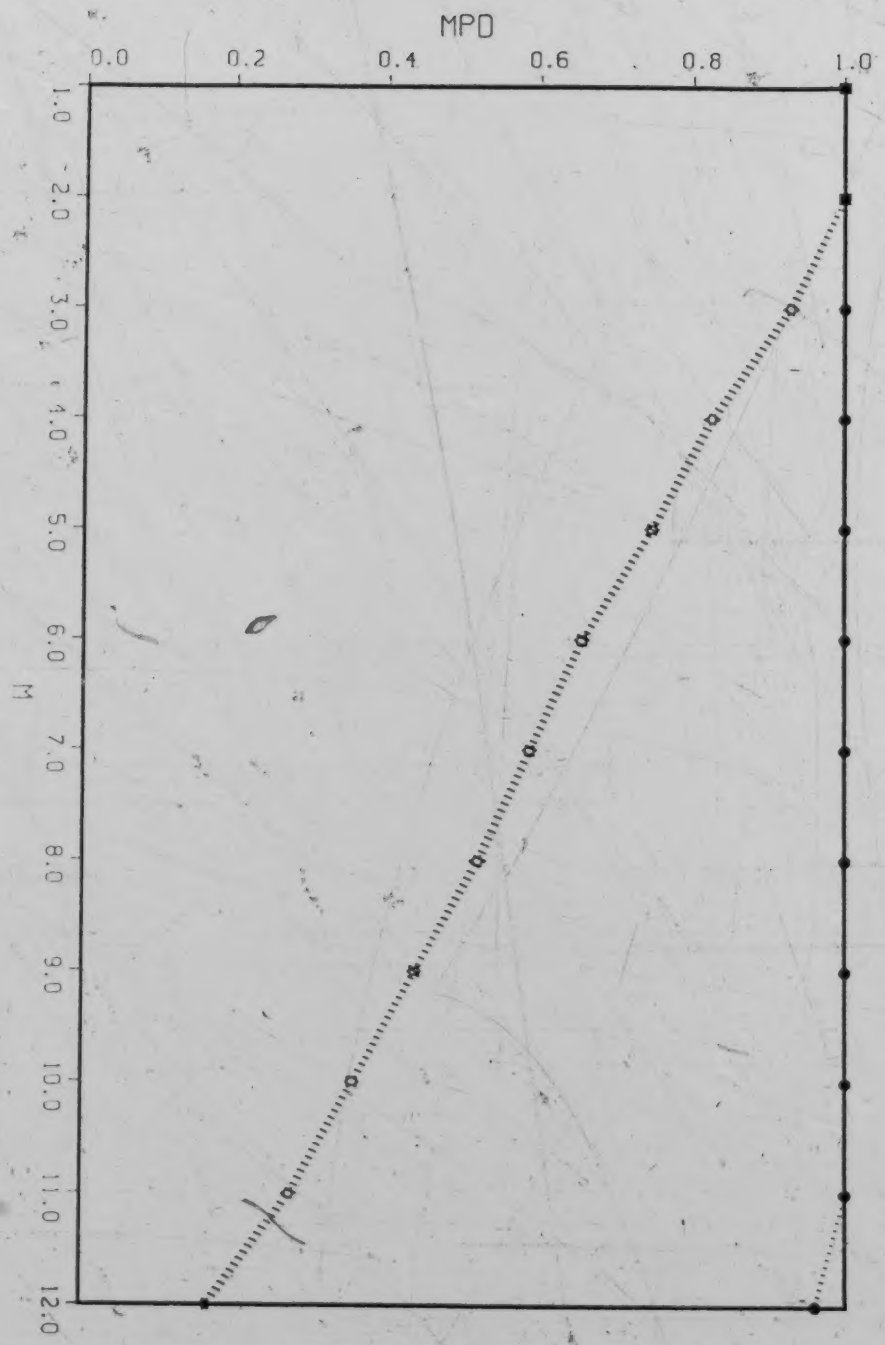

Fig.5.5 Typical MPDs at 0.1, 5 and 7.5mm along the sensor parameterized by dot, upward triangle and downward triangle respectively.

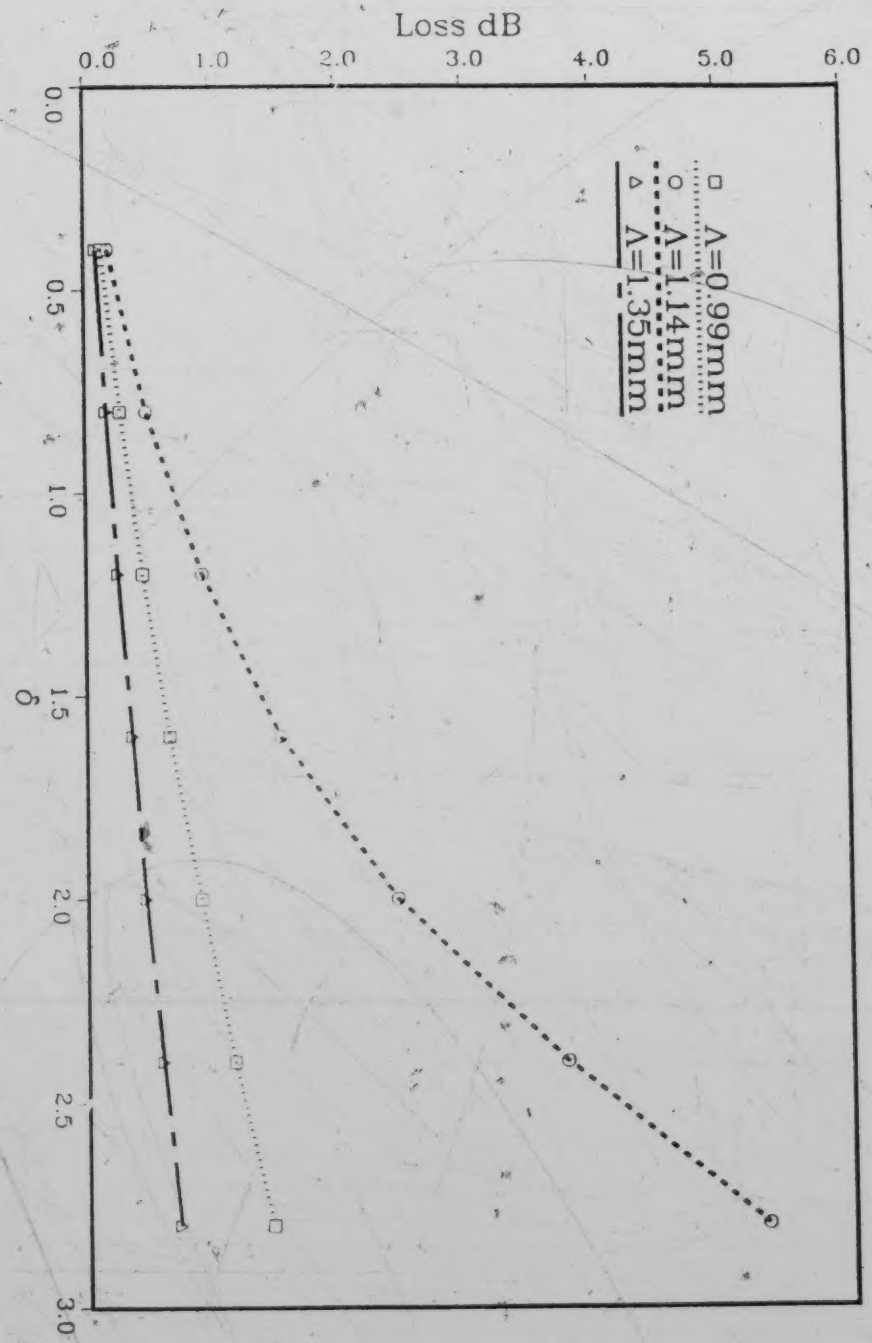

Fig.5.6 Typical plot of loss versus amplitude of the sensor.

parameterized by the period of the sensor.

increases rapidly as the ray period equals the sensor period. This phenomenon will be discussed in Section (5.3.3).

In practice, the force causing the variation in the sensor amplitude is the only measurable quantity. Thus a relation between the force and the sensor amplitude is of paramount importance. Such a relation is derived in [11] and is also given below

$$F = (148.6\ b^4\ E\ L\ \delta) / \Lambda^4 \quad (N) \qquad (5.10)$$

where b is the diameter of the fiber including cladding, E is the Young's modulus of elasticity for the fiber, L is the length of the sensor, Λ and δ are the period and the amplitude of the sensor respectively and F is the force (measured in Newtons) causing the variation of the sensor amplitude. For example, a force of F=4.25N is required to produce a deformation amplitude of δ=5μm with a period Λ=1.43mm and the total length of L=10 Λ with E= 7 $10^{10} N/m^2$.

5.3.3 EFFECT OF CHANGE IN MICROBENDING PERIOD ON POWER LOSS

The procedure for calculating this effect is as follows. The conventional fiber of Section (5.3.2) is used. The sensor amplitude is fixed at δ=1μm. Initially the value of the sensor period is set to a value well below the ray period (Λ=0.9mm). Rays carrying equal powers are launched at the input of the sensor according to the scheme introduced in Chapter 2 and the loss is determined at a distance of 8mm along the sensor. This procedure is repeated many times and every time the period of the sensor is incremented by 20μm, until the value of the sensor period is well above the value of the ray period. The result is

presented in Fig.5.7. From figure 5.7 it is evident that power loss increases as the value of the sensor period approaches the value of the ray period and attains a maximum value when the sensor period equals the ray period. Beyond this point power loss decreases as the sensor period further increases. This feature of the microbending sensors is called resonance [51]. A mathematical analysis of the ray equations also confirms the resonant property of the sensor. This analysis can be done by setting $W = Q + \varepsilon$ in Eq.(5.7) with ε being very small. Retaining the first order terms in ε and using the approximation $\sin(\varepsilon Z) \simeq \varepsilon Z$ and $\cos(\varepsilon Z) \simeq 1$, Eq.(5.7) reduces to

$$Y(Z) = Y_o \cos(Q_1 Z) + (k_{yo}/n_1 k_o Q)\sin(Q_1 Z) + (\Gamma/2Q_1)Z\sin(Q_1 Z) \qquad (5.11)$$

The amplitude of the last term in Eq.(5.11) is a linear function of the distance Z along the fiber's length. Knowing that

$$r(Z) = \left[X^2(Z) + Y^2(Z) \right]^{1/2} \qquad (5.12)$$

Equation (5.11) shows that even for very small amplitudes, every ray will eventually be lost if the sensor is long enough.

5.4 SERIAL MICROBENDING SENSORS

Microbending sensors have been widely used for the measurement of pressure [13], sound level [14,15], displacement [16] and structural distortion [17]. An experimental study of the performance of sensors in series has been described by Mickelson et al [51]. He came to the conclusion that the loss at a given sensor is independent of the loss at

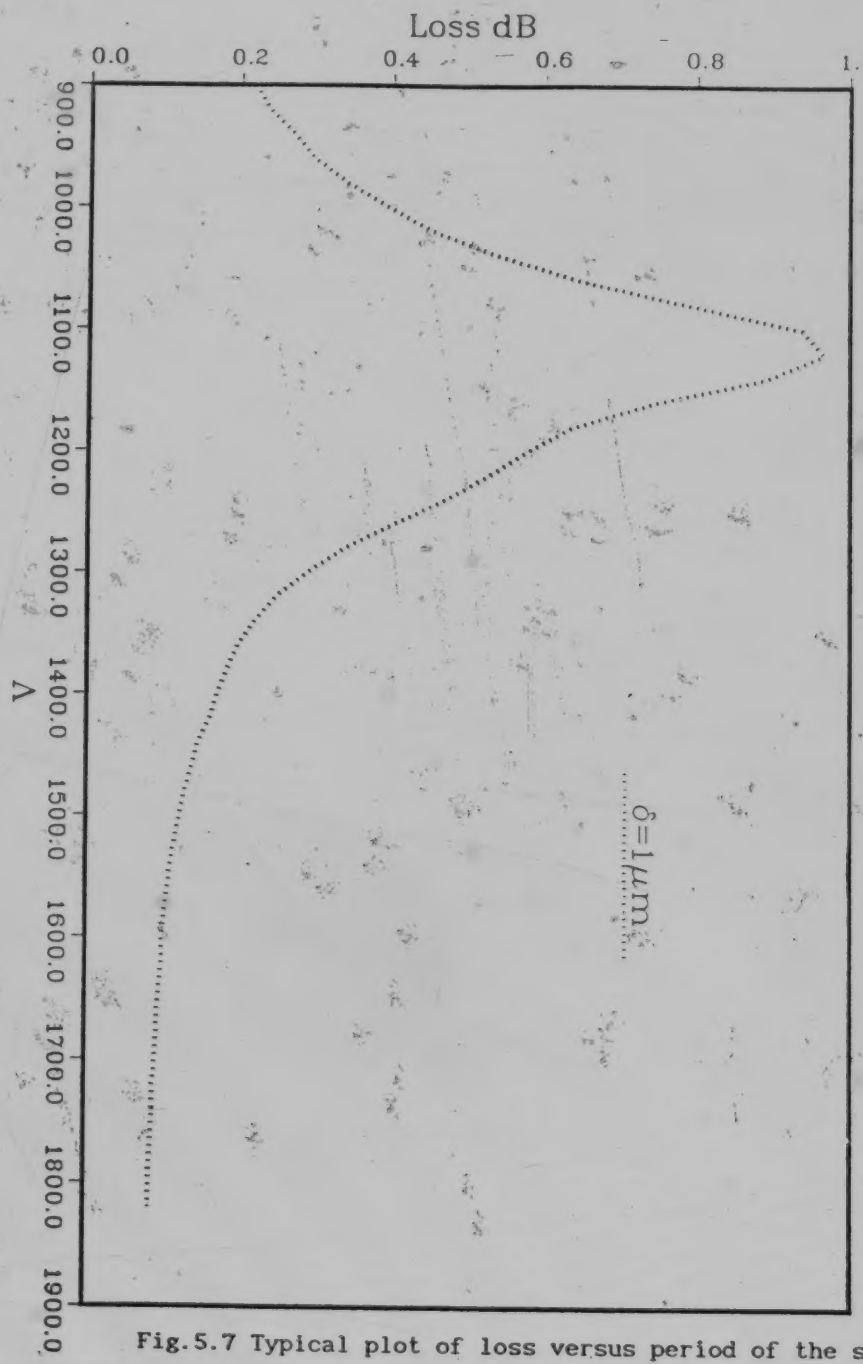

Fig.5.7 Typical plot of loss versus period of the sensor.

other sensors. In the same paper, he attempts to provide an explanation for the loss characteristic of a sensor using a mode number diffusion model. However, in this Chapter attempt is made to duplicate the same results using ray tracing. In particular the case of two sensors in series where the performance of the second sensor (downstream sensor) may depend on the performance of the first sensor (upstream sensor). Although there are practical ways of analyzing the performance of two sensors in series such as the backscattering technique [51], a theoretical approach based on the ray theory is presented here.

The main focus of this section is on the performance of the second sensor while the first sensor is subjected to amplitude variations. A schematic diagram of two sensors in series is given in Fig 5.8. The unperturbed fiber length l is the separation distance between the two sensors and normally much greater than the length of the sensors in order for the modal power distribution to reach steady state. In our case however, where the only source of mode coupling is the geometrical perturbation of the fiber, the modal power distribution in the straight fiber is constant. Therefore, the length of the straight fiber l is immaterial for achieving a steady state modal power distribution and may be chosen to be in the order of one ray period. The procedure for determining the loss along the length of the two sensors is as follows. Using a conventional fiber and setting the periods and the lengths of both sensors to be equal i.e $\Lambda_1=\Lambda_2=1.5$mm and $L_1=L_2=20$mm respectively and $l=20$mm. Initially, the amplitude of the first sensor is set to $\delta_1=3\mu$m and the amplitude of the second sensor is set to $\delta_2=4\mu$m. As in Chapter 2, rays are launched into the input of the first sensor and the power loss is determined at every 200μm along the sensors and the unperturbed

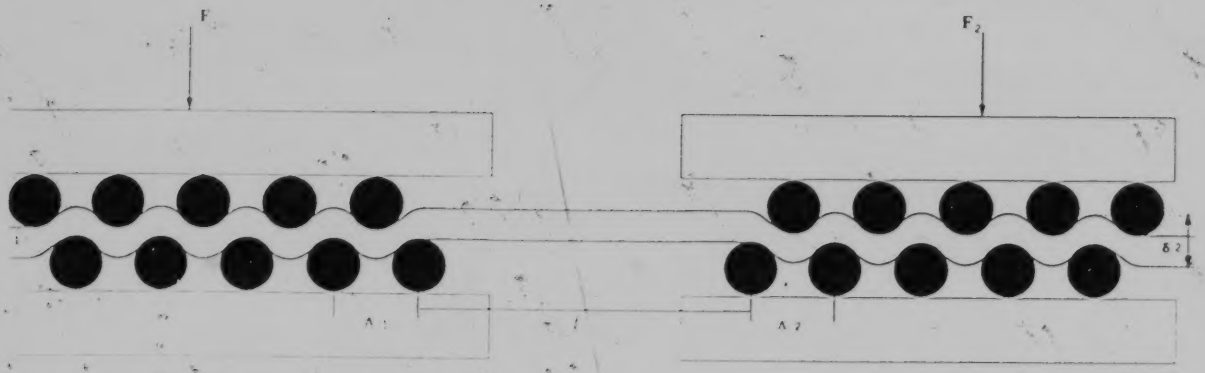

Fig.5.8 Schematic diagram of two sensors in series

section of the fiber separating the sensors. This procedure is repeated for δ_1 = 3, 4, 5, 6μm. The result is given in Fig.5.9.

A peculiar property of serial sensors can be inferred from Figure.5.9. That is, the magnitude of the loss at the second sensor is nearly constant for any loss at the first sensor. Thus, one can conclude that the loss at the second sensor is almost independent of the loss at the first sensor. This characteristic behavior of the serial sensors determined by ray tracing is in agreement with the experimental results obtained in Reference [51]. This characteristic of the serial sensors is depicted in Fig.5.10, where the change in the loss at the second sensor ΔP_2 is plotted against the loss at the first sensor P_1. This figure shows negligibly small change in the magnitude of the loss at the second sensor as the loss in the first sensor varies. This result may be employed for practical purposes where a number of sensors are used in series. It means that the reading from one sensor will not be influenced by the conditions at another upstream sensor.

The result obtained in this section seems to contradict the mode stripping property of the sensor where higher order modes are eliminated. Now a question may be posed: if the higher order modes are eliminated in the first sensor, then why should there be loss at the second sensor? The answer to this question lies in the basic property of induced mode coupling by microbending sensors. As a ray propagates through a sensor, its mode number fluctuates rapidly and the range of fluctuation depends on the ray's initial condition. Therefore a ray which has not been lost in the first sensor may easily be lost in the second sensor.

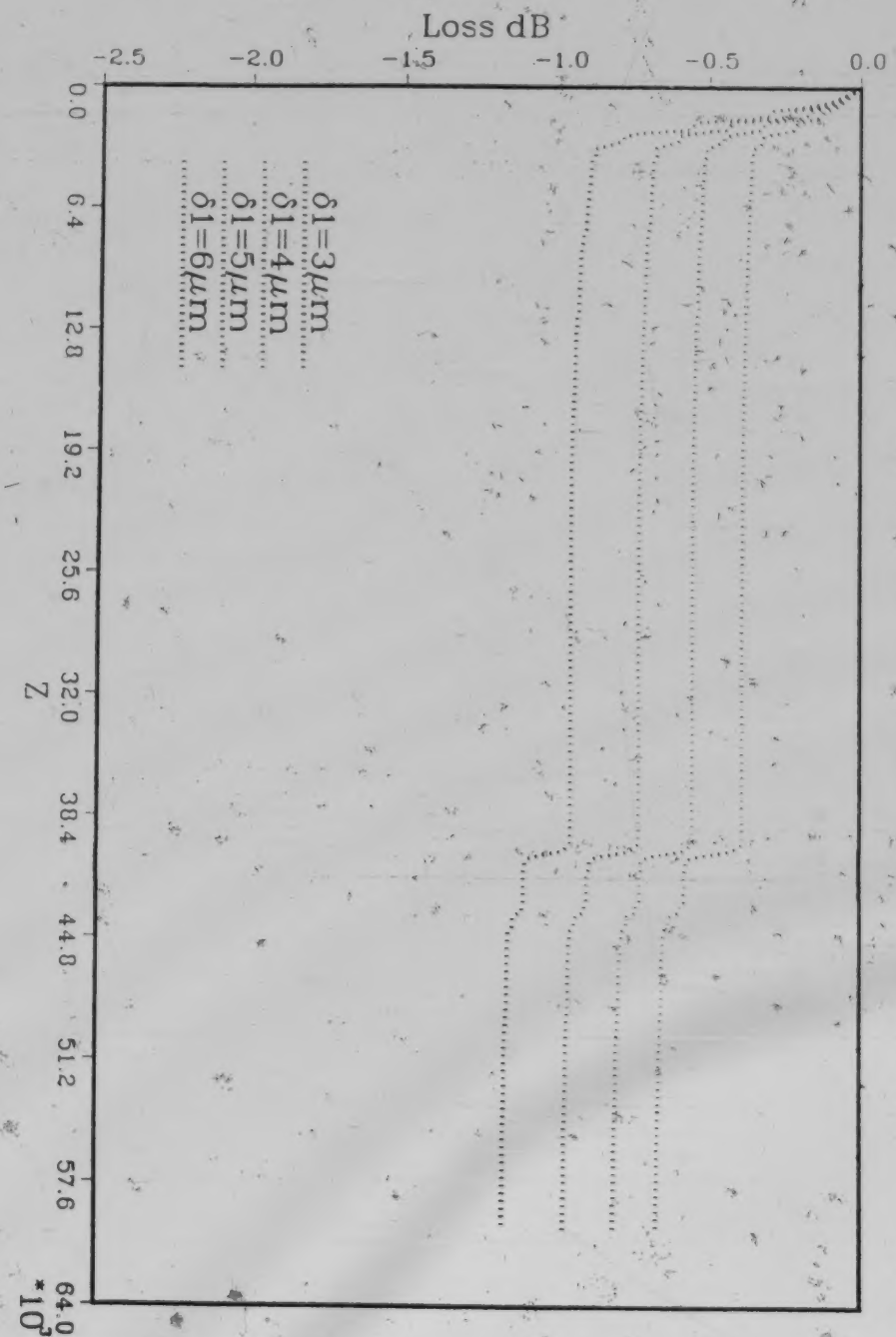

Fig.5.9 Typical loss versus distance along the two sensors parameterized by the amplitude of the first sensor.

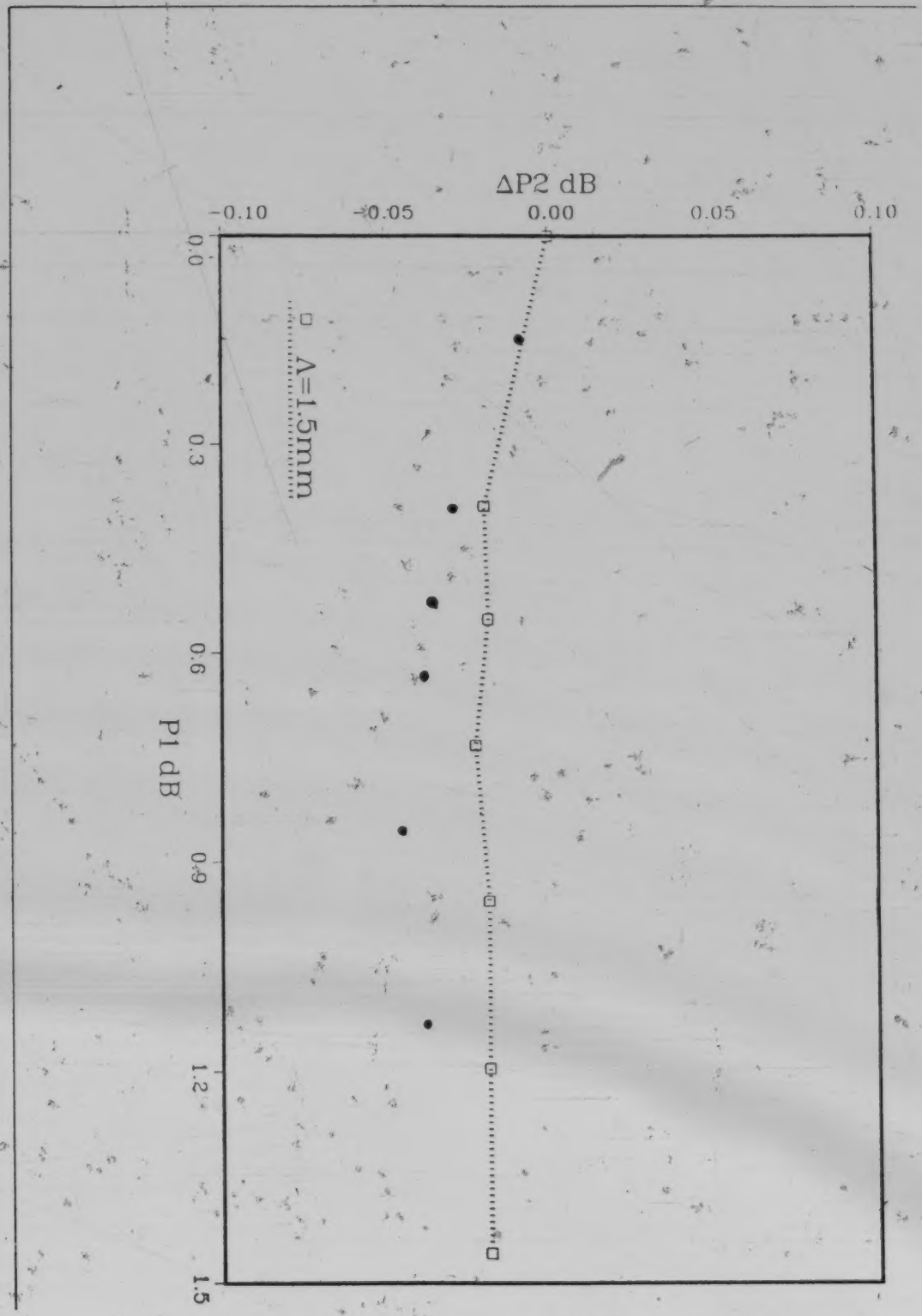

Fig.5.10 Plot of the change in the loss at the second sensor as a function of loss at the first sensor.

CHAPTER 6

SUMMARY

The primary concern of this thesis is the determination of power attenuation characteristics of mode dependent optical fiber components. A matrix method is introduced which enables us to determine the loss of optical power from multimode optical fiber components taking into account DMA. This method is based on the linear expansion of each mode group power at the output in terms of the powers of all the mode groups at the input. The coefficients of the expansion form a matrix called the T-matrix. The T-matrix provides information about mode group coupling coefficients, modal power distribution, DMA, and total loss.

Implementation of this technique in the analysis of two fiber connectors leads to highly accurate results which are in good agreement with theoretical and experimental results obtained by other authors namely C.M.Miller [36] and G.Evers [7]. The plot of transmission versus lateral offset shows a gradual decay in the transmission as the lateral offset increases and finally reaches zero as the lateral offset reaches twice the fiber core radius. A comparison of Fig.3.3 with Fig.3.7 indicates that fiber connectors with lateral offset and angular misalignment exhibit identical loss characteristics. This is explained by the fact that the phase space volume occupied by the excited mode groups in a graded index fiber exhibit a rotational symmetry. The T-matrix technique is then employed in the analysis of graded index bent fiber taps. The characteristic behavior of loss versus the distance along the bend clearly shows the regions where radiation and tunnelling

losses dominate. It should be mentioned that for fibers with different parameters the amount of radiation loss and tunnelling loss differ. Furthermore, the amount of loss depends on the radius of curvature of the bend. The larger the radius of curvature the smaller the loss will be. The MPD obtained from the T-matrix further confirms the mode stripping property of the bent fibers. The plot of MPD indicates that higher order modes are eliminated from the fiber core as the rays advance along the bend. A comparison of the loss versus the distance characteristic of the bend with that of Reference [50] shows good agreement. However, in Reference [50] the point where radiation loss ceases and tunnelling begins occurs at a longer distance along the bend compared to the point obtained in this thesis.

Finally, the study of microbending sensors is carried out by assuming a sinusoidal deformation of the fiber core with certain amplitude and period. The equations of motion for the rays are derived and the solutions to the equations of motion are determined. Again the T-matrix is used for the characterization of the sensors. The curve of loss versus the distance along the sensor indicates that radiation loss dominates up to a distance of few sensor periods along the sensor. Beyond this distance the loss is strictly due to tunneling. The periodic fluctuations along the curve of loss versus the distance is indicative of the fact that radiation and tunnelling losses occur at those points where the periodic radius of curvature of the sensor is the smallest. The MPD curve shows the mode stripping property of the sensor, where higher order modes are gradually eliminated from the core as the rays advance along the sensor. The MPD finally attains a steady state and gradually decreases.

The solutions to the ray equations in a sensor predict a resonant behavior where the ray period equals the sensor period. At resonance the positions of the rays from the fiber axis increases as the rays advance along the sensor. The curves of loss versus the sensor amplitude shows that at resonance the loss increases more rapidly with respect to change in the amplitude of the sensor than at non-resonance. The resonant property of the sensor is shown in the plot of loss versus the period of the sensor. This plot indicates an increase in the loss as the sensor period approaches the ray period and attains a maximum when the sensor period equals the ray period.

The study of the performance of two serial sensors was considered next. In this analysis emphasis has been put on the performance of the downstream sensor while the upstream sensor is subjected to amplitude changes. The curves of loss versus the distance along the sensors and the straight section of the fiber separating the two sensors show that, regardless of the amount of loss at the first sensor the amount of loss at the second sensor remains constant. This result leads to an important conclusion concerning serial sensors, that is, the amount of loss at a given sensor is independent of the loss at the upstream sensors.

The study of serial sensors concludes this research project, however, there are more questions to be addressed in analyzing the performance of mode dependent optical fiber components. For future research we suggest that the performance of the above optical fiber components be analyzed using different MPDs at the input. The T-matrix approach may be used to analyze the performance of couplers and tapers. Finally microbending sensors may be analyzed using the propagating beam method.

References

[1] A.H.Cherin, "An Introduction to Optical Fibers. New York: McGrow-Hill Book Company, 1983.

[2] R.L.Galawa, G.E.Chamberlin, G.W.Day, D.L.Franzen and M.Young National Bureau of Standards, Electromagnetic Technology Division, National Engineering Laboratory.

[3] R.Olshanski, S.M.Oaks,"Differential mode attenuation measurements in graded-index fiber," Applied Optics, Vol.17, No.11, pp.1830, 1978.

[4] G.Evers, "Calculation and measurement of mode transition matrices for differential mode attenuation and differential mode delay characterization of optical fibers," Optical engineering, Vol.27, No.2, pp.179, 1988.

[5] A.R.Mickelson and M.Eriksrud, "Mode-dependent attenuation in optical fibers," J.Opt.Soc.Am., Vol.73, No.10, pp.1282, 1983.

[6] D.Marcuse, Principels of Optical Fiber Measurements. New York: Academic Press, 1981.

[7] G.Evers, "Mode transition matrices for fiber-optic connectors," Electtronics Letters, Vol.21, No.9, pp.401, 1985.

[8] M.Y.Loke, "Non-introsive optical fiber tapping," M.Sc Thesis, University of Alberta.

[9] C.Miller, "Connectorless taps for coated single mode or multimode optical fibers," European Conference on optical communications, 21-24 September 1982, Cannes, France.

[10] A.K.Agarwal, U.Unrau, "Comparative study of methods to produce stationary mode power distribution for optical fiber measurements," J.Opt.Commun., Vol.4, No.4, pp.126, 1983.

[11] H.F.Taylor, "Bending effects in optical fibers," J.Lightwave Technology, Vol.LT-2, No.5, pp.617, 1984.

[12] M.Eriksrud, A.R.Mickelson and S.Lauritzen, "Backscattering signatures from optical fibers with differential mode attenuation," J.Lightwave Technology, Vol.LT-2, No.2, pp.139, 1984.

[13] J.N.Fields, C.K.Asawa, O.G.Ramer, and M.K.Barnoski, "Fiber optic presure sensor, " J.Acoust.Soc.Amer., Vol.67, pp.816, 1980.

[14] J.N.Fields and J.H.Cole, "Fiber microbend acoustic sensor," Appl.Opt.,Vol.19, pp.3265, 1980.

[15] N.Lagakos, W.J,Trott, T.R.Hickman, J.H.Cole, and J.A.Bucaro, "Microbend fiber optic sensor as extended hydrophone," IEEE J.Quantum Electron., Vol.QE-18, pp.1633,1982.

[16] N.Lagakos, T.Litovitz, P.Macedo, R.Mohr, and R.Meister, "Multimode optical fiber displacement sensor," Appl.Opt., Vol.20, pp.167, 1981.

[17] C.K.Asawa, S.K,Yao, R.C.Stearns, N.L.Mota, and J.W.Downs, "High sensitivity fiber optic strain sensors for measuring structural distorsion," Electron.Lett., Vol.18, pp.362,1982.

[18] M.Born and E.Wolf, principles of Optics, 3rd edition, Pergamon Press, New York, 1964

[19] A.Z.Capri, Nonrelativistic quantum mechanics. California: The Benjamin/Cummings Publishing Company, Inc.,1985.

[20] R.L.Liboff, Introductory quantum mechanics.California: Holden-day Inc., 1980.

[21] D.Marcuse, Light Transmission Optics. New York: Van Nostrand Rienhold Company Inc., 1982.

[22] A.W.Snyder and D.J.Michell, "leacky rays on circular optical fiber," J.Opt.Soc.Amer., Vol.64, No.5, pp.599, 1974.

[23] A.W.Snyder, D.J.Michell, and C.Pask, "Failure of Geometrical Optics for Circular Optical Fibers," J.Opt.Soc.Amer., Vol.64, No.5, pp.608, 1974.

[24] J.D.Jackson, Classical Electrodynamics. New York: John Wiley and Sons, 1975.

[25] J.R.Ritz, F.J.Milford, and R.W.Christy, Fundamentals of Electromagnetic Theory, Addison-Wesley Publishing Company, 1980.

[26] J.Arnaud, Hamilton theory of beam mode propagation, Progress in Optics XI, Ed.E.Wolf, North Holand 1973.

[27] H.Goldstein, Classical Mechanics, California: Addison-Wesley Publishing Company, 1980.

[28] J.B.Marion, Classical Dynamics, New York: Academic Press, 1970

[29] S.Berdague and P.Facq, "Mode division multiplexing in optical fibers," Appl. Opt., Vol.21, pp.1950, 1982.

[30] P.Facq and P.Fournet, "Observation of tabular modes in multimode graded index optical fiber," Elect.Lett., Vol.16, pp.648, 1980.

[31] A.R.Mickelson, M.Eriksrud, "Mode-dependent Attenuation in optical fibers," J.Opt.Soc.Amer., Vol.73, No.10, pp.1282, 1983.

[32] G.Evers, A.Kober, and Undo Unrau, "Measurement of mode transition matrices of quasi-step-index optical fiber components," in Fiber Optics: Short-Haul and Long-haul Measurements and Applications II, R.L.Galawa, ed., Proc.SPIE 500, pp.94, 1984.

[33] S.Piazola, G.De Marchis, "Analytical relations between mode power distribution and near-field intensity in graded index fiber," Electron.Lett., Vol.15, No.22, pp.721, 1979.

[34] Y.Daido, E.miyauchi, T.Iwama, and T. Otsuka, "Determination of modal power distribution in graded index optical wave guides from near-field patterns and its application to differential mode attenuation measurement," Appl.Opt., Vol.18, pp.13,1979.

[35] G.T.Holms, "Estimation of concatinated system response based on measured transfer functions for low and high order modes," in Proc. 7th European Conf. on Optical Communication (Copenhagen), pp.3.4-1 - 3.4-4, Peter Peregrinus, London 1981.

[36] C.M.Miller "Transmission vs Transvers offset for parabolic -profile fiber splices with unequal core diameter," Bell System Technical Journal, Vol.55, No.7, pp.917, 1976.

[37] A.H.Cherin, P.J.Rich, "Amulti-groved embossed plastic splice connector for joining groups of optical fiber," Appl.Opt., Vol.14, pp.3026, 1975.

[38] C.M.Miller, "Loose tube splices for optical fibers," B.S.T.J., Vol.54, pp.1215, 1975.

[39] C.M.Miller, "A fiber optic cable connector,"B.S.T.J, Vol.54, pp.1547, 1975.

[40] Dr.J.N.McMullin, University of Alberta, Private communication, 1988.

[41] D.Gloge, "Offset and tilt loss in optical fiber splices," Bell System Technical Journal, Vol.55, No.7, pp.905,1976.

[42] L.Lewin, "Radiation form curved dielectric slabs and fibers," IEEE Trans. Microwave Theory Tech., Vol.MTT-22,pp.718,1974.

[43] J.A.Arnaud, "Transverse coupling in fiber optics, Part III:Bending losses," Bell Syst.Tech.J., Vol.53, pp.1379, 1974.

[44] E.F.Kuester and D.C.Chang, "Surface-wave radiation loss from curved dielectric slabs and fibers," IEEE J.Quantum Electron., Vol.QE-11, pp.903, 1975.

[45] A.W.Snyder, I.White, and D.J.Mitchell, "Radiation from bent optical wave guides," Electron.Lett., Vol.11, pp 311, 1975.

[46] D.Marcuse, "Curvature loss formula for optical fibers," J.Opt.Soc.Amer., Vol.66, pp.216, 1976.

[47] D.Marcuse, " Field deformation and loss caused by curvature of optical fibers," J.Opt.Soc.Amer., Vol.66, pp.311, 1976.

[48] J.Sakai, "Simplified bending loss formula for single-mode optical fibers," Appl.Opt., Vol.18, pp.951, 1976.

[49] Dr.J.N.McMullin, University of Alberta, Private communication, 1989.

[50] C.Winkler J.D.Love, and A.K.Ghatak, "Loss calculations in bent multimode optical waveguides," Opt.Quantum Electron.,

Vol.11, pp.173, 1979.

[51] A.R.Mickelson, ϕistein Klevhus, and M.Eriksrud, "Backscatter readout from serial microbending sensors," J.lightwave Tech., Vol.LT-2, No.5,pp.700, 1984.

[52] J.N.Fields, "Attenuation of parabolic index fiber with periodic bends," App.Phys.Lett., Vol.36, pp.799, 1979.

[53] D.Marcuse, "Losses and impulse response of a parabolic index fiber with random bends," Bell Sys.Tech.J., Vol.52, pp.1423, 1973.

[54] L.T.Wood and F.Romero-Borja, "Optical attenuation by periodic microdistorsions of a sensor fiber," Opt.Lett., Vol.10, No.12, pp.632, 1985.